Msc thesis in Mechanical Engineering

Decoding the Wavelet Puzzle: Finding the Champion Mother Wavelet for Joint Impedance System Identification

by

Lambert Ren

Student number: 5509823

Examination Committee:	Prof. Alfred Schouten
	Dr. Mark van de Ruit
	Prof. Manon Kok
Date of defense:	September 7th, 2023

Delft University of Technology

Netherlands

September 2023

Decoding the Wavelet Puzzle: Finding the Champion Mother Wavelet for Joint Impedance System Identification

Lambert Ren*
supervised by Prof. Alfred Schouten[a] and Dr. Mark van de Ruit[a] .

***Abstract*—To have a better understanding of difference in characteristics between various mother wavelets, this paper presents a comprehensive investigation into the performance of three commonly used non-orthogonal mother wavelets, namely Morlet, Paul and DOG, in a wavelet-based system identification approach when used for evaluating joint impedance. This method is further modified to make the estimation result much closer to the realistic result. Additionally, the optimization of smoothing parameters is explored across ten distinct situations, encompassing diverse stiffness waveforms such as step, square, sine, triangle, and sawtooth, as well as two different input perturbations. Performance metrics, including running time, random error, bias error, total error, and variance accounted for (VAF), are used to assess the performance of the system identification method in each scenario. The result shows that Paul wavelet yields a better result of stiffness estimation together with bias error for most situations after averaging. The DOG has the shortest running time and Morlet wavelet gives the highest VAF and lowest random and total error. The findings of this study contribute to a better understanding of the strengths and weaknesses of various mother wavelets in joint impedance estimation, providing valuable insights for future applications in the field of system identification and parameter estimation in neuromechanics control.**

***Index Terms*—Wavelet transform, mother wavelets, system identification, parameter estimation, human joint impedance**

I. Introduction

Using time series (TS) is a useful method for exploring the fluctuations and changes in variables [1]. In the field of neuromechanics control, several techniques have been applied to time series data to characterize the joint's mechanical properties of a time-varying system [2]. The joint impedance of a system can be defined as a metric that expresses the dynamic relationship between an externally applied joint displacement and the corresponding restoring joint torque, which is a good quantification of the joint's mechanical properties, shown as Fig. 1 [3]. System identification methods have been extensively employed to explore these mechanical properties during different postural tasks and under varying experimental conditions [3]. There exists lots of time-varying system identification methods aiming to the identification of joint impedance [2]. There are various system identification (sysID) techniques available for analyzing time series data, which can be broadly categorized into three types based on their domains: time domain, frequency domain, and a combination of both time and frequency domains [4]. For example, the short data segment (SDS) is a time-domain method [5], while the ensemble spectral method (ESM) is based on frequency domain [6].

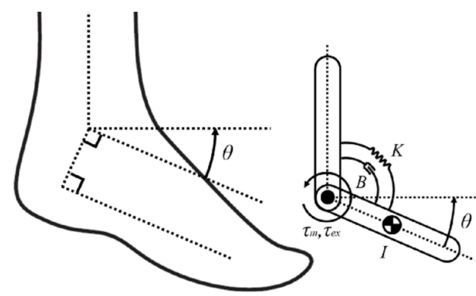

Fig. 1. Dynamic model of human ankle joint.

Moreover, a time-frequency domain based method has been developed for the identification of joint admittance making use of the wavelet transform (WT) [7]. This is the first time of applying wavelet transform for the identification of joint impedance and this method demonstrates promising outcomes in estimating the mechanical properties of human joint. WT can be used to decompose a time series into the time-frequency space, which makes it possible to identify the dominant modes of variability and understand how these modes change over time [8]. The method makes use of WT to transfer the time signals into a time-frequency representation. The cross wavelet transform (XWT) has been applied to find the relationship between the input perturbation angle and the output torque, which will be lately served as the non-parametric identification result. The joint impedance parameters will be derived from this result using the nonlinear least square method.

Great care is needed when applying WT in this method since that all the possible factors, such as the selection of mother wavelets, parameter in mother wavelets' equations and the scale parameters, could affect the result [9]. In WT, the mother wavelets are finite-length waveforms that are scaled and translated to analyze the signal [10]. Different mother wavelets, such as Morlet and Paul wavelets, can be selected for specific applications, each with its own characteristics and properties.

* Master student at TU Delft, The Netherlands.
[a] Laboratory for Neuromuscular Control, Department of Biomechanical Engineering, Delft University of Technology, Mekelweg 2, Delft 2628CD, the Netherlands.

A. Problem statement

There are multiple parameters that need to be carefully selected and considered during the execution of this wavelet-based system identification method. This paper mostly focuses on the results obtained from applying different mother wavelets, specifically concerning various time-varying systems. This study is carried out based on the wavelet package developed by Christopher Torrence and Gilbert P. Compo, which has been implemented for the analysis conducted in their research [8]. Particular attention was given to the three commonly used non-orthogonal mother wavelets in this study, namely the Morlet wavelet, the Paul wavelet and the Derivative of Gaussian (DOG) wavelet. Morlet wavelet has a better frequency localization, while Paul exhibits a better localization in time and DOG wavelet is only composed of real part [9]. Considering these distinct properties exhibited by these mother wavelets, five time-varying systems are being applied to assess the performance and results of the method. These systems are distinguished by different joint stiffness, specifically including non-periodic step waves, periodic square waves, sine waves, triangle waves, and sawtooth waves.

B. Goal

The goal of this study is to assess and compare the variations in parameter estimation results when employing different mother wavelets, namely Morlet, Paul and DOG wavelet, in the wavelet-based system identification method for diverse time-varying systems, including non-periodic step waveform, periodic square, sine, triangle and sawtooth waveforms, in simulation.

C. Outline

This paper develops further investigation on the selection of different mother wavelets for system identification method in various scenarios. The paper is organized as follows: Section 2 gives an introduction to this wavelet-based system identification method, the wavelet transform and mother wavelets used in this study. A simulation is performed, serving as a basic comparison between these three mother wavelets. Section 3 first introduced the open-loop human joint impedance model, following by the simulation environment used in the later experiment, introducing the system to be identified and parameters used for simulations. Section 4 shows how to optimize the result of this wavelet-based sysID method, by making modifications and adding more constraints to the process and finding the optimal parameter sets used in the following simulations. In Section 5, parameter estimation results in various scenarios are presented with the conclusion of best mother wavelet to be used under that situation. In Section 6, some extension experiments have been introduced to give more guidance and suggestion on the use of this wavelet-based method. Finally, the report is summarized with a discussion about the future work and conclusion of the study.

II. Wavelet

This section introduces some fundamental concepts and background knowledge on which this study is based, including the wavelet transform, mother wavelets to be discussed in this paper. A simulation result is also included to briefly compare the different characteristics of these mother wavelets. Finally, the wavelet based system identification method is introduced at the end of this section.

A. Wavelet transform

The wavelet transform (WT) of a function $f(t)$ is defined as the convolution of $f(t)$ with a mother wavelet $\psi(\eta)$, which is given by [9]:

$$W = \int_{-\infty}^{\infty} f(t)|a|^{(-\frac{1}{2})}\psi^*(\eta)dt, \tag{1}$$

where ψ^* is the complex conjugate of the mother wavelet $\psi(\eta)$ and a is the scale parameter can only be set larger than 0. The η is generally set to

$$\eta = \frac{t-b}{a}, \tag{2}$$

where b is the time shift factor which can determine the temporal location in time. Similar to the Short-time Fourier transform (STFT), wavelet transform can be viewed as the projection of a signal into a set of basis functions named wavelets [11]. The difference between them is that the wavelet transform can change the length of window by adjusting the value of scale, however, the window length in STFT is fixed initially and therefore has limitations on non-stationary time series analysis [12].

In practical applications, various types of wavelet transforms are used for different use, employing numerous kinds of mother wavelets.

B. Mother wavelets

To optimize efficiency, it is preferable to use mother wavelet functions that are continuously differentiable and compactly support [13]. The wavelet functions are in generally both absolutely and square integrable, which means they have to satisfy the following equations,

$$\int_{-\infty}^{\infty} |\psi(\eta)|dt < \infty \tag{3}$$

$$\int_{-\infty}^{\infty} |\psi(\eta)|^2 dt < \infty \tag{4}$$

Furthermore, there are also many other wavelet properties of mother wavelets, such as progressive and linear phase, good localization in time or frequency, a trade-off between time and scale, complex or real, and the property of being orthogonal or not [14]. In this study, the performance of three orthogonal mother wavelets provided by Torrence and Compo's code is looked into to evaluate their effectiveness when dealing with different time-varying system, namely Morlet, Paul and Derivative of Gaussian (DOG) [15]. They are respectively defined as [9],

$$\psi(\eta) = \pi^{-1/4}e^{-\eta^2/2}e^{ik\eta}, \tag{5}$$

$$\psi(\eta) = \frac{2^k i^k k!}{\sqrt{\pi(2k)!}}(1 - i\eta)^{-(k+1)}, \tag{6}$$

$$\psi(\eta) = \frac{(-1)^{k+1}}{\sqrt{\Gamma(k + \frac{1}{2})}} \frac{d^k}{d\eta^k}(e^{-\eta^2/2}). \tag{7}$$

which should be inserted into Equation 1.

The parameters of these three mother wavelets used in this study stick to the empirically derived factors from Torrence's guide., where k are separately set to 6, 4 and 6 [8]. The plots of real parts of these mother wavelets are shown as Fig. 2.

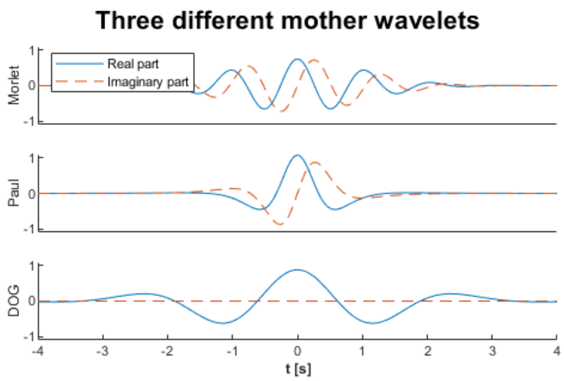

Fig. 2. The three different mother wavelets, from top to below, separately Morlet, Paul and DOG, while the key parameter setting to 6, 4 and 6. The real part is plotted with a solid line and the imaginary part is plotted with a dashed line.

C. A brief comparison between mother wavelets

As introduced in the Section 2.B, this study will specifically examine the effect brought by three different mother wavelets provided by Torrence and Compo's wavelet transform package. Their plots of both real parts and imaginary parts are separately shown in Fig. 2. Moortel pointed out the characteristics of the three mother wavelets with a short experiment about the wavelet transform of a time-varying frequency signal: the Morlet wavelet exhibits good frequency resolution, the Paul wavelet demonstrates superior time localization, and the DOG wavelet falls somewhere between the other two in terms of performance. [9]. In order to demonstrate the basic differences among these three mother wavelets described by Moortel, this study reproduces his simulation with the same analytical function as mentioned in his paper, with the form of

$$f(t) = \begin{cases} sin(2\pi 10t), & 0 \leq t < 1/4, \\ sin(2\pi 25t + \frac{\pi}{2}), & 1/4 < t < 1/2, \\ sin(2\pi 50t - \frac{\pi}{2}), & 1/2 < t < 3/4, \\ sin(2\pi 100t + \frac{\pi}{2}), & 3/4 < t \leq 1. \end{cases} \tag{8}$$

The plots for this analytical signal is shown in Fig. 3.

In order to provide a more comprehensive demonstration of the analysis results for different mother wavelets within the wavelet package provided by Torrence, the simulations in this section are based on the code available in that package. This package is preferred over using function provided by MathWorks, as it has been found out to produce results with slight differences. Relying on this wavelet package code allows for more precise conclusions to be drawn as a fundamental assumption, considering that all subsequent simulations conducted in this study also rely on this package. The wavelet transform result of the signal are given in Fig. 3. To be mentioned, the k parameters within Morlet, Paul and DOG mother wavelets are also separately set to 6, 4 and 6, which is stick to the value introduced previously.

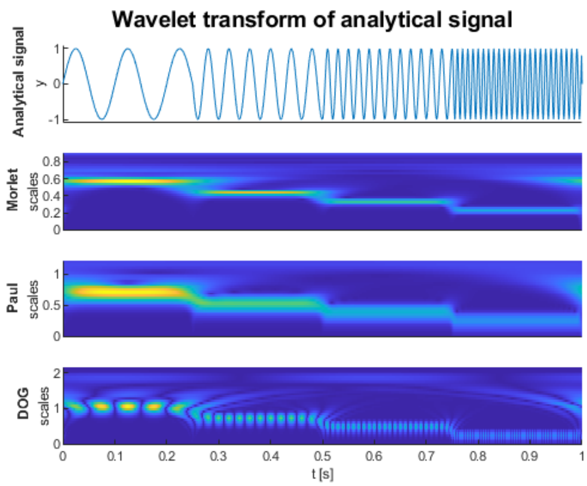

Fig. 3. The wavelet transform result of the analytical signal used in Moortel's paper. The top figure shows the signal to be analyzed, the other three plots from top to bottom are separately the result when using mother wavelet Morlet, Paul and DOG in WT. The result is based on the wavelet package developed by Torrence.

It can be seen that for the result using Morlet mother wavelet, yellow triangles exhibit the narrowest width, which corresponds to the values on the scales, which means the good frequency resolution. But there are higher noise for the length of triangles, which corresponding to the time. In opposite, the result triangles of Paul mother wavelet have neater length but broader width. This just proves the conclusion mentioned above: Paul wavelet demonstrates superior time localization. However, for the result plot of DOG mother wavelet, the triangles are split into several blocks. Both the widths and lengths of the triangles for the DOG mother wavelet fall in between the performance of the other two mother wavelets. In the meantime, yellow triangles are surrounding by noise of various shapes. While, there seems to have the largest confidence interval in the background of DOG mother wavelet's figure with less noise.

The simulation study results presented here offer an opportunity to establish a fundamental assumption for subsequent simulations involving various time-varying systems. Based on these results, certain expectations can be set for the performance of different wavelets. The use of Morlet wavelet is expected to provide better estimations of the exact values of the system parameters. It is expected to yield more precise results when estimating the true values of the system. On the other hand, the Paul mother wavelet is expected to outperform in scenarios where there are sudden changes or discontinuities at specific time steps. Finally, the DOG mother wavelet may introduce more noise in the estimation results. These expectations and assumptions provide valuable insights for guiding and interpreting future simulations involving different time-varying systems and selecting appropriate wavelets for system identification. Additionally, the DOG wavelet is expected to exhibit the least effect resulting from boundary effects, making it more reliable in capturing the desired features near the edges of the data.

III. Simulation study

This section provides a detailed description of the simulation study conducted to assess the performance of mother wavelets on various time-varying systems. To begin with, the human joint impedance model will be introduced. The parameters used in this simulation model, different waveforms to be identified and also two different kinds of input perturbation will be discussed in the following parts.

A. Human joint impedance model

In this study, a simplified time-varying open loop human joint impedance model was chosen to be used in the simulation study, which was shown in Fig. 4. This model is commonly used in a force task experiment, where participants react to angular perturbations. As a consequence, the joint torque will also exhibit time-varying characteristics [16]. This model exactly describes the relationship between the angular input $u(t)$, torque output $y(t)$ and measurements noise n(t) [2]. The model is described by:

$$y(t) = H_{joint}(s,t)u(t) + n(t), \tag{9}$$

where $H_{joint}(s,t)$ is a 2nd-order inertia-spring-damper system with a time-varying stiffness, which can be described by:

$$H_{joint}(s,t) = Is^2 + Bs + K(t), \tag{10}$$

where I is the inertia of the joint, B is the viscosity of the joint and $K(t)$ is the time-varying stiffness of the joint, s is the Laplace variable equals to $j2\pi f$.

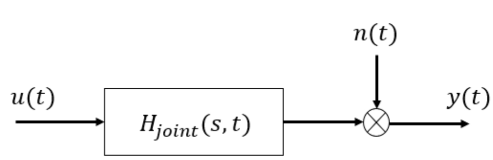

Fig. 4. The simplified time-varying open loop human joint impedance model with angular input $u(t)$, torque output $y(t)$ and measurements noise n(t).

B. Simulation parameters and perturbation signal

1) Simulation parameters: The model used in this study was implemented in MATLAB 2019b-Simulink 9.7 [2]. The chosen parameters in $H_{joint}(s,t)$ which introduced in Eq. 4 were employed to represent the impedance of the human ankle joint in a seated position. Joint inertia and viscosity will be set to time-invariant during this study . The study employed commonly selected parameter values, where inertia is set to 0.02 $Nm.s^2/rad$ and viscosity is set to 2.2 $Nm.s/rad$ [17].

Given that this study focuses on evaluating the performance of different mother wavelets on systems with varying waveforms, the joint stiffness $K(t)$ in Eq. 4 is separately described by step, square, sine, triangle and sawtooth waves. In general, non-periodic waves do not display a repeated pattern over time, making them more unpredictable compared to periodic waves. Among these waveforms, a step function can be considered as a representative example of a non-periodic waveform, it consists of an instantaneous change from one level to another, and this transition occurs abruptly and does not exhibit any oscillation or fluctuation [18]. And all the other waveforms are simple examples of periodic waveforms. And they can effectively represent various significant shapes in common signals observed in nature, such as sudden drops/rises, smooth oscillations and ramp shape patterns [19]. The square wave demonstrates an abrupt and instantaneous transition between two levels. The sine wave exhibits a smooth, continuous, and symmetric oscillation. The triangle wave displays a linear and symmetric rise and fall. While the sawtooth wave is a combination of an abrupt fall and a linear rise. These different shapes allow for a further investigation into the effectiveness of this system identification method using different mother wavelets.

For the non-periodic step function, the stiffness amplitudes is set to be changing from 100 Nm/rad to 150 Nm/rad, with a duration time of 10 s. For the square wave, sine wave and sawtooth wave, the stiffness ranges from 50 Nm/rad to 150 Nm/rad, with a duration of 40 s and frequency 0.1 Hz [2]. For the triangle wave, the stiffness ranges from 100 Nm/rad to 150 Nm/rad, so that it has the same slope as the sawtooth wave. The figure of waveforms to be identified is shown in Fig. 5.

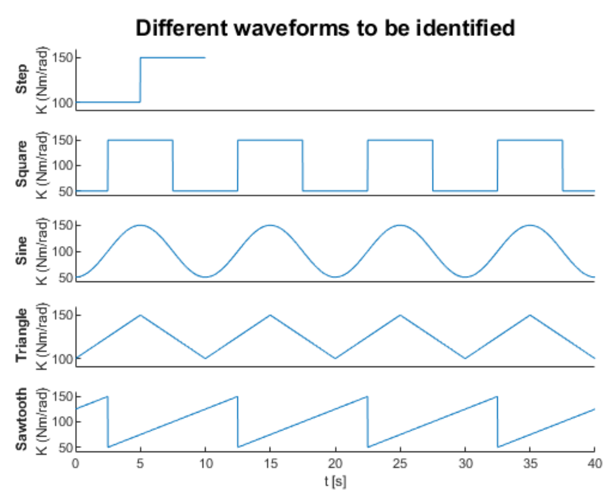

Fig. 5. Different joint stiffness $K(t)$ to be identified in this simulation study. From top to bottom, figure shows the step wave, square wave, sine wave, triangle wave and sawtooth wave separately.

To simulate the sampling process, the frequency of time series is downsampled by a factor of 1/10. As a result, the frequency of the time series from which the parameters are extracted is 100 Hz.

The output noise, which is denoted as $n(t)$ in Eq. 9 is a normally distributed noise signal that has been low-pass filtered with a 2nd-order Butterworth filter, with a cutoff frequency of 40 Hz. In order to ensure that the noise has a desirable effect on the output signal, the amplitude of output noise was adjusted such that the signal to noise ratio (SNR) of the resulting output signal of the simulink model is 10 dB [20]. Examples of the different angular input perturbations $u(t)$ and their corresponding output torques $y(t)$ both with noise and without noise for a step system are shown in Fig. 6.

Moreover, in order to reduce the influence of randomness in the simulation, experiments are repeated 100 times for all the different mother wavelets across various time-varying system.

2) Perturbation signal: Two commonly used perturbation input signals, denoted as $u(t)$, were used as inputs to the system. The first input signal is a filtered noise signal that has been passed through a second-order Butterworth low-pass filter with a cutoff frequency of 5 Hz. It has a mean absolute velocity of 0.20 rad/s. The second input signal is a pseudo-random binary sequence (PRBS) signal with a switching rate of 147 ms and a mean absolute velocity of 0.08 rad/s. Both signals were scaled such that they had a root mean square (RMs) of $0.5\deg$ (0.0087 rad). Moreover, a small trick filter module was used to extract velocity and acceleration data from the filtered position before sending the input perturbation into the joint impedance simulation system.

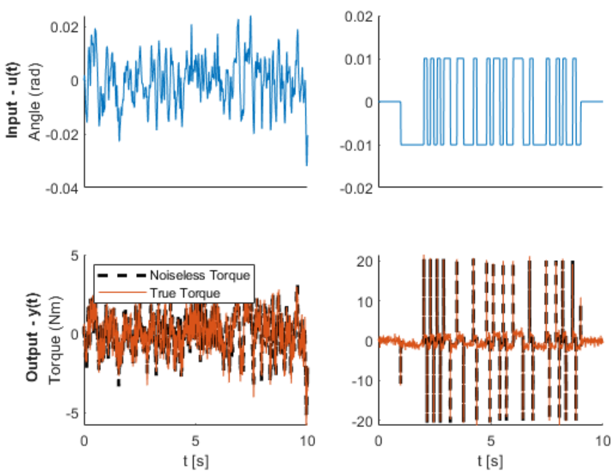

Fig. 6. The angular input to the model is either a 5 Hz low-pass filtered noise $u_1(t)$ or a pseudorandom binary sequence $u_2(t)$. The noiseless torque and true torque output of the model are both shown in the second line of the figure, where noiseless torque is plotted with a thick black dotted line and true torque with thin solid line.

C. Wavelet based system identification method

The method under investigation in this study is mainly developed based on the cross wavelet transform (XWT) of the provided time-series data, which is a system identification method developed in 2009 as a part of MSc thesis [7]. The whole process of this method is shown in Fig. 7. To begin

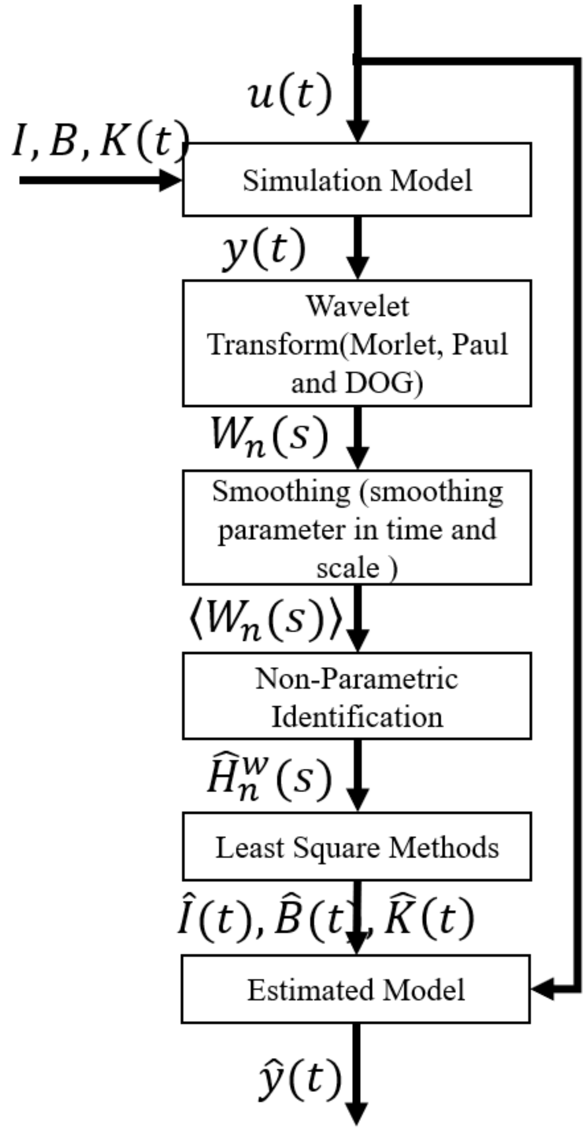

Fig. 7. Scheme of the method. $u(t)$ is the input perturbation to the simulation model. I, B, $K(t)$ is separately the initial inertia, viscosity and stiffness, where $K(t)$ is time-varying. $y(t)$ is the output torque of the simulation model. The spectral density results $W_n^{YU}(s)$ and $W_n^{UU}(s)$ can be calculated using the cross wavelet transform, and there are three mother wavelets, Morlet, Paul and DOG to be chosen from in this study. $\langle W_n^{YU}(s)\rangle$ and $\langle W_n^{UU}(s)\rangle$ are separately the smoothing result of the spectral density results, during which smoothing parameters in time and scale should be selceted. After smoothing, the estimated transfer function $\hat{H}_n^w(s)$ can be calculated. With this estimated transfer function, estimated parameters can be approximated with least square methods fitting transfer function onto the Eq. 10. With these new parameters, a estimated model was built. Finally, the estimated output torque $\hat{y}(t)$ can be calculated with the same input perturbation $u(t)$ to the estimated model.

with, XWT is used for measuring the similarity between two waveforms. It is defined as follows,

$$W_n^{UY}(s) = W_n^U(s) W_n^{Y*}(s) \tag{11}$$

where U and Y separately refer to the Fast Fourier Transform (FFT) of the two time-series, $u(t)$ and $y(t)$, and $*$ is the complex conjugation [8].

After the application of the cross wavelet transform on the time-series, the obtained spectral density results are smoothed in order to decrease the variance of the estimator. The smoothing process is performed in both the time domain and the frequency domain, following the form:

$$\langle W_n^{UY}(s)\rangle = S_{scale}(S_{time}(W_n^{UY}(s)) \tag{12}$$

where S_{scale} represents the smoothing carried out along the wavelet scale axis, and S_{time} denotes the smoothing in time axis. In this study, these two parameters are defined as follows:

$$S_{time}(W_n)|_s = (W_n(s) * e^{-\frac{n^2}{2(s/sdt)^2}})|_s \tag{13}$$

$$S_{scale}(W_n)|_n = (W_n(s) * \Pi((\delta j_0/sdj)s))|_n \tag{14}$$

where sdj and sdt are the smoothing factors separately in scale and time. Hereby in this study, a Gaussian function is used for smoothing in time, and a boxcar function is employed for smoothing in scale. These smoothing operators are in a similar form with the mother wavelets discussed in this paper. According to Torrence and Combo, the parameter δj_0 is separately set to 0.6, 1.5 and 0.97 for Morlet, Paul and DOG mother wavelets [8]. This smoothing method represent an optimal compromise between time and scale [15].

Similar to the frequency response of systems based on the Fourier transform, the time-varying frequency response function (FRF) can be defined as:

$$H_n^w(s) = \frac{W_n^{YU}(s)}{W_n^{UU}(s)}. \tag{15}$$

An estimate with a lower variance can be achieved using a smoothed result described in the Equation 12:

$$\hat{H}_n^w(s) = \frac{\langle W_n^{YU}(s)\rangle}{\langle W_n^{UU}(s)\rangle}. \tag{16}$$

By showing the equation of estimated system admittance, denoted as $\hat{H}_n^w(s)$, it represents the transfer function between the input perturbation angle and the output torque. To extract additional information about joint mechanics from the transfer function, least squares method is applied to fit the transfer function onto the time-varying model of human joint impedance $H_{joint}(s,t)$. With the help of this method, one can determine the parameter values that minimize the sum of the squares of the differences, or residuals, between the fitting function and the experimental data [21]. The estimated value obtained through this method have been proved to have the highest probability (maximum likelihood) of being accurate, provided that certain critical assumptions are valid.

Finally, a new estimated human joint impedance system can be built based on this result. With the same input, the estimated torque $\hat{y}_{est}(t)$ can be calculated, which can be compared with the true torque to evaluate the effectiveness of the method used.

D. *Performance quantification*

To evaluate and compare the performance of the method using different mother wavelets across various systems, six metrics were selected to calculate the result of the simulation study [2]. They are separately bias error, random error, total error, running time, variance-accounted-for (VAF) and rise time.

1) Bias error: Bias error, also known as systematic error, is used to calculate the error in the average parameter estimation result obtained from the repeated times' experiments with respect to the true joint stiffness [22]. It is defined as:

$$Err_{bias} = \sqrt{\frac{\triangle t}{T}\sum_{i=1}^{T/\triangle t}(\bar{\hat{K}}(i\triangle t) - K(i\triangle t))^2}, \tag{17}$$

where $K(i\triangle t)$ is the true joint stiffness and $\bar{\hat{K}}(i\triangle t)$ is the average estimated stiffness across all the 100 trials at time point $i\triangle t$. Bias error generally provides a better interpretation about an inaccurate estimation of the system identification method.

2) Random error: Random error is used to calculate the variance of the estimated stiffness across different simulation trials over the 100 repeated times [5]. It is defined as:

$$Err_{random} = \sqrt{\frac{\triangle t}{R\cdot T}\sum_{i=1}^{T/\triangle t}\sum_{r=1}^{R}(\hat{K}(i\triangle t, r) - \bar{\hat{K}}(i\triangle t))^2}, \tag{18}$$

where $\hat{K}(i\triangle t, r)$ is the stiffness estimated at $i\triangle t$ in the r-th trial. In this method, the parameter estimation result always remains the same for the same perturbation input $u(t)$, the same output torque $y(t)$ and the same parameters. It will be proved in the later sections. Therefore, the random error is mostly concerned with the variations in input perturbations $u(t)$ and noise $n(t)$. Consequently, random error can provide a better assessment of the method's robustness using different mother wavelets.

3) Total error: Total error is a combination of both the systematic error and random error, this describe the overall error in the system identification of the joint stiffness. It is defined as:

$$Err_{total} = \sqrt{\frac{\triangle t}{R\cdot T}\sum_{i=1}^{T/\triangle t}\sum_{r=1}^{R}(\hat{K}(i\triangle t, r) - K(i\triangle t))^2}. \tag{19}$$

This can be used to find the measurement of error between the estimates obtained from all the 100 trials and the true stiffness waveforms.

4) Running time: The running time refers to the average duration taken to complete the system identification process from the input perturbation $u(t)$ and the output torque $y(t)$. This can show the effectiveness of the method when applying different mother wavelets.

5) Variance-accounted-for: VAF describes the goodness of fit of the time domain identification procedures [23]. It can be defined as:

$$VAF(i\triangle t) = (1 - \frac{E[(y(i\triangle t) - \hat{y}(i\triangle t))^2]}{E[y(i\triangle t)^2]}) \cdot 100\%, \quad (20)$$

where $y(i\triangle t)$ is the noiseless true torque at time point $i\triangle t$, $\hat{y}(i\triangle t)$ is the estimated torque at time point $i\triangle t$ using the parameters received from system identification. E is the expectation. VAF can be used to assess the extent to which the time-varying model of joint impedance explains the output torque data [2].

6) Rise time: Rise time generally refers to how rapidly a time-varying system identification method can adjust to an abrupt change in simulated stiffness [2]. This is quantified by examining the derivative of the estimated stiffness, and special attention should be paid to the time point where the true stiffness undergoes a sharp change.

IV. Optimizing simulation result

To better align the estimated results with the realistic situation and yield the advantages of performance for each mother wavelets, a brief optimization was conducted on both the method process itself and the parameters used within the method before the simulation.

A. Performance metrics used in optimizing

Given that the previous performance metrics were designed for situations where simulations are repeated multiple times which mostly cost hours to perform the simulation for a single scenario, this section introduces new performance metrics only for this part to accommodate a single optimization process. They are separately root mean square error (RMSE), mean absolute error (MAE) and standard deviation (SD) between the estimated stiffness and true stiffness.

1) Root mean square error: RMSE describes the average difference between the estimated value and the actual value, it is defined as [24],

$$RMSE = \sqrt{\frac{\triangle t}{T}\sum_{i=1}^{T/\triangle t}(\hat{K}(i\triangle t) - K(i\triangle t))^2}. \quad (21)$$

2) Mean absolute error: MAE a more natural measure of average error comparing to RMSE, it is defined as [25],

$$MAE = \frac{\triangle t}{T}\sum_{i=1}^{T/\triangle t}|\hat{K}(i\triangle t) - K(i\triangle t)|. \quad (22)$$

3) Standard deviation: SD mainly introduces the degree to which how estimated result points cluster around the mean value, it is defined as [26],

$$SD = \sqrt{\frac{\sum_{i=1}^{T/\triangle t}(\hat{K}(i\triangle t) - K(i\triangle t))^2}{T/\triangle t}}. \quad (23)$$

These three indicators will serve as crucial reference metrics for the subsequent optimization process in this section.

TABLE I
THE LOWER BOUNDS AND UPPER BOUNDS OF ALL PARAMETERS FOR LEAST SQUARE METHOD IN BOTH TWO TRIALS

	First trial		Second trial	
	Lower bound	Upper bound	Lower bound	Upper bound
Inertia $(Nm.s^2/rad)$	0	0.1	$\bar{\hat{I}}_{estimated}$	$\bar{\hat{I}}_{estimated}$
Viscosity $(Nm.s/rad)$	0	10	0	10
Stiffness (Nm/rad)	0	1000	0	1000

B. Optimize the parametric estimation

According to Kearney, the inertia parameter in the human ankle typically characterized by small positive values with a very low variance [3]. To get a constant estimated inertia, the least square method is performed twice. In the first trial, the estimated inertia $\hat{I}(t)$ is averaged across time to obtain $\bar{\hat{I}}_{estimated}$. This value is then set as the inertia parameter and remains unchanged during the second iteration of the least square method, a condensed version of the scheme including major modification is shown in Fig. 8. With this slight modification, the estimation result of the inertia parameter will remain constant and have a positive value. Meanwhile, to ensure that the results fall within a realistic range, lower and upper bounds are applied to both trials. These values are listed in Table I.

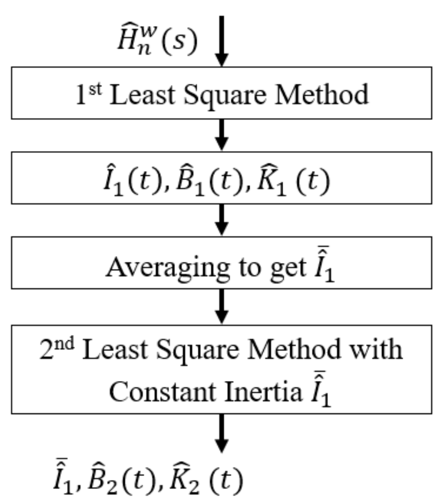

Fig. 8. Scheme of the modifications to the method. All the other processes will be exactly the same as shown in Fig. 7. The first parameter estimation will be performed given the transfer function $\hat{H}_n^w(s)$. The estimated time series of inertia $\hat{I}_1(t)$ will be averaged to $\bar{\hat{I}}_1(t)$. During the second least square method, the inertia will be set to the constant $\bar{\hat{I}}_1$. The final result of the parameter estimation will be separately $\bar{\hat{I}}_1$, $\hat{B}_2(t)$, $\hat{K}_2(t)$.

An example result of the modified method is given in Fig. 9. The model used in this example is the periodic square wave, and the mother wavelet used here is Morlet. The smoothing parameters are set to 10 for both in time and scale. It can be observed from the figure that all three estimated results, inertia, viscosity and stiffness, fall within the feasible range for the human ankle joint in real-life scenarios. Furthermore, the estimated inertia remains constant over time, while the viscosity exhibits slight variations, which are acceptable for human joints, except for the beginning and ending parts that are significantly influenced by boundary effect [27].

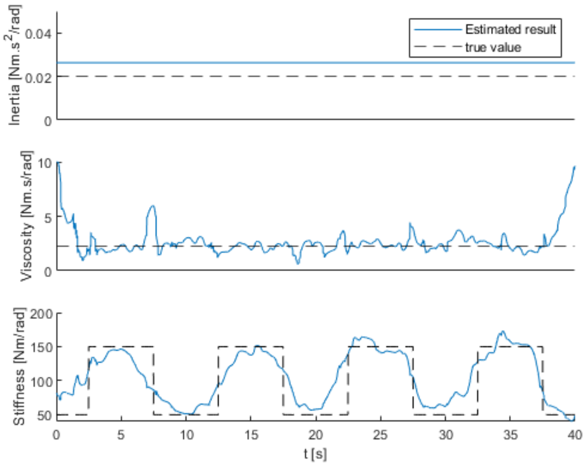

Fig. 9. The estimated result of the method after the modification introduced is plotted with blue line and the true value is plotted with black dotted line. The system to be identified is the periodic square wave the mother wavelet used here is Morlet. Both the smoothing parameters in time and scale are set to 10.

Meanwhile, the new method exhibits increased robustness to the choice of the starting point for the least square method. The performance metrics, RMSE, MAE and SD with respect to the true stiffness exhibit only slight variations according to the initial stiffness value, as illustrated in Fig. 10. Considering the actual experimental scenario, it is more likely that the approximate value is not known in advance. This further validates the practicality of this modified method. Therefore, all the subsequent simulation experiments carried out in this study will be based on this modified method. To be mentioned, the initial point of all the subsequent simulation experiments will be set to $p_0 = [0.02; 2.2; 100]$.

C. Optimize the smoothing parameters

In Eq. 13 and Eq. 14, there are two smoothing factors sdt and sdj separately in time and scale. Use of these two parameters have great effect on the system identification result since they will greatly affect the non-parametric identification result $\hat{H}_n^w(s)$. Therefore, it will also have significant variations in the parameter estimation results for different smoothing parameter sets. An example comparison between different smoothing parameter set is given in Fig. 11. The results indicate an inverse relationship between the smoothing effect and the values of the smoothing parameter sets. When the parameters are set to $sdt = 0.1$ and $sdj = 0.1$, the result is over smoothed since that the estimated stiffness value deviate significantly from the true value of the system. However, the estimated viscosity seems to have a better approximation to the true system with lower variation. When the parameters are set to $sdt = 10$ and $sdj = 10$, the estimated stiffness seems to successfully detect the initial system resembling a square system.

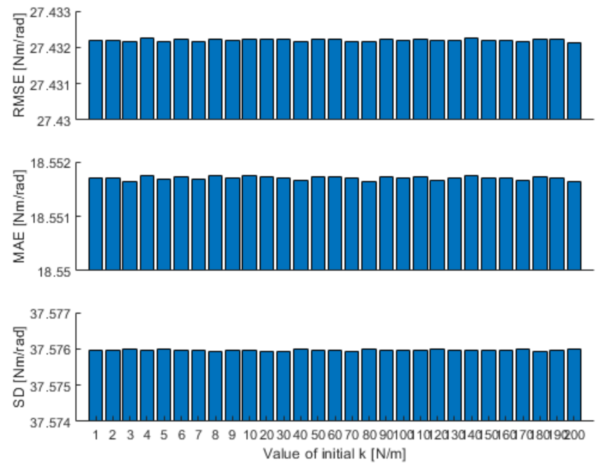

Fig. 10. Performance metrics of the estimated stiffness exhibit only slight variance with respect to the initial stiffness value set as the starting point of the stiffness. The system to be identified and all the parameters used remain consistent to those used in Fig. 9.

However, the result seems to be under-smoothed especially for the viscosity, which should ideally be a constant value. In the following parts of this section, preliminary experiments are performed to determine the optimal smoothing parameter sets for each scenarios, aiming to better illustrate the advantages and characteristics of different mother wavelets in this system identification method.

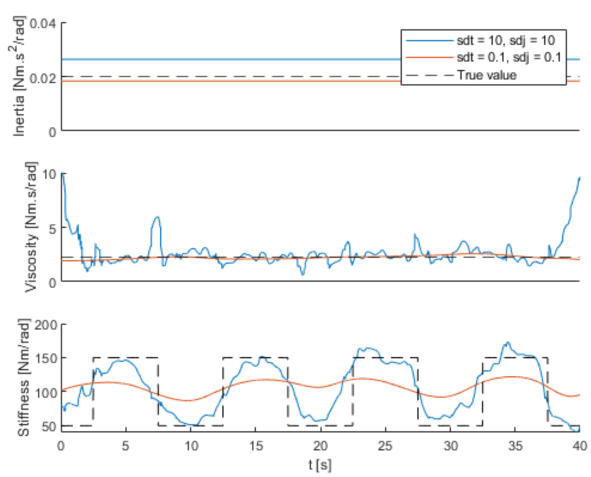

Fig. 11. Comparison between different smoothing parameter sets for a square system using Morlet wavelet. The true value is plotted as black dotted line. When setting both parameters to 10, the result is plotted with blue solid line. When setting both parameters to 0.1, the result is plotted with red solid line.

To further investigate the optimal combination of these two parameters, a preliminary simulation was conducted. During this simulation, both smoothing parameters will be considered within the range of 0.1 to 10. The parameter values will be sampled at intervals of 0.1 from 0.1 to 1, and at intervals of 1 from 1 to 10. The performance metrics for this simulation are again selected as RMSE, MAE and SD. The simulation was carried out for method using all the mother wavelets mentioned on various systems with different perturbation inputs. A particular example result is given in Fig. 12 and Fig. 13. Since that there are two variables affecting the result, two plots with different ways of clustering bars are presented. In this way, these plots can better illustrate to what extent either parameters are affecting the result of the system identification.

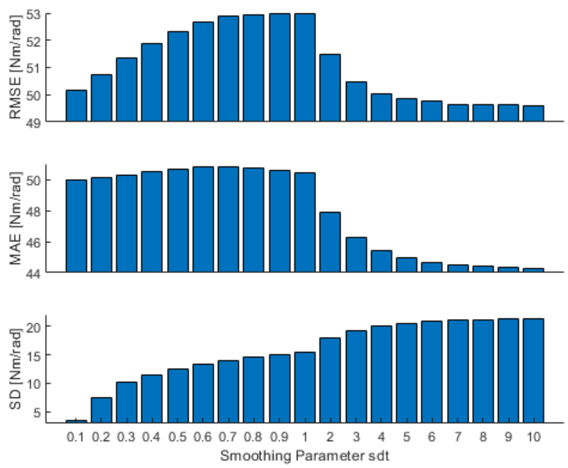

Fig. 12. Performance metrics of the step system (PRBS input) using Morlet wavelet with different smoothing parameter in time sdt, while setting smoothing parameter in scale $sdj = 1$.

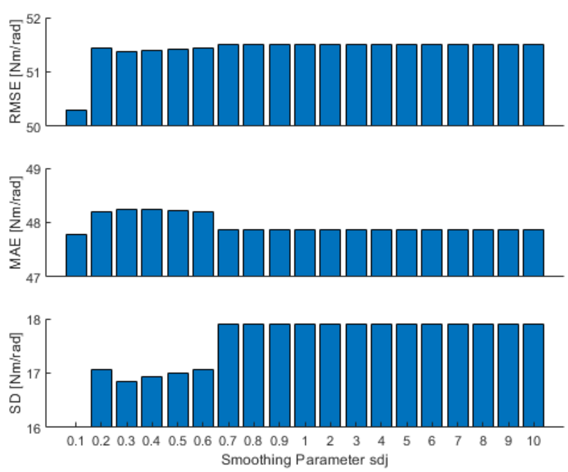

Fig. 13. Performance metrics of the step system (PRBS input) using Morlet wavelet with different smoothing parameter in scale sdj, while setting smoothing parameter in time $sdt = 1$. Comparing with the Fig. 12, performance metrics show smaller variations when smoothing parameter in time sdt is set to constant.

It can be seen from these two plots that the smoothing parameter in time has a much more significant influence on the result of estimated stiffness. When the performance metrics are clustered with constant sdj, great difference can be detected from the lowest valley to the highest peaks. When the the performance metrics are clustered with constant sdt, resulting shape of the plot closely resembles a square. It has been proved that this is not an coincidence, as similar results have been observed for each mother wavelet and various fixed smoothing parameter values, different perturbation inputs, and all the introduced systems discussed earlier. Therefore, a better sdj will be first selected to simplify the process. For the example given here, $sdj = 0.1$ is selected, and only smoothing parameter in time will be investigated in the following part of this section.

To better select from these parameters, sparse figures have been plotted with varying sdt. In these figures, only the values that exhibit significant changes compared to their neighbours will be presented. All the parameter values not included are either have a rather close value to its neighbours or follow the same trend, either increasing or decreasing, as their neighbour values. A typical example is given in Fig. 14.

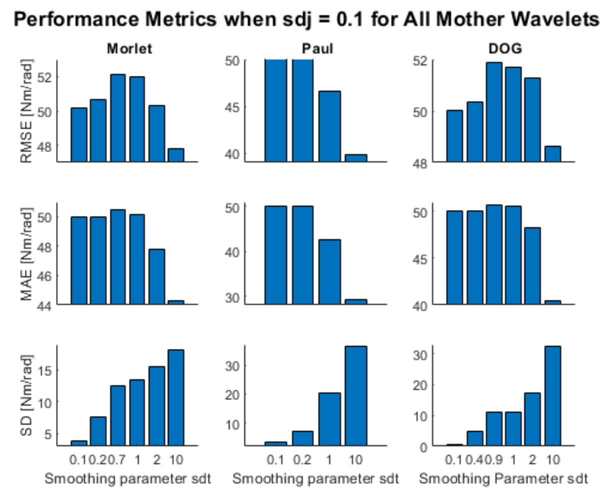

Fig. 14. Performance metrics of the step system (PRBS input) for all mother wavelet while selecting $sdj = 0.1$. Only those parameter values with unique results are presented in this figure.

To better show the difference between estimated inertia, viscosity and stiffness for different smoothing parameters, the estimated result is shown in Fig. 15.

Based on the estimated results and the performance metrics, a final optimal parameter set will be selected. There are two principles for selecting the final parameter used for repeated system identification simulation. The first principle is that the estimated stiffness should be as close to the value as possible. Furthermore, preference will be given to the results with lower variance compared to those with higher variance, considering that the system being identified in this study primarily consists of a smooth time series. In the example scenario, $sdt = 0.2$ is chosen for further analyzing because of several reasons. In Fig. 14, it can be observed that among all the values presented, the value of 0.2 yields the lowest RMSE and MAE. Additionally, the SD value associated with this parameter seems acceptable. And in Fig. 15, result associated with the value of 0.2 has a faster rise time comparing to that of 0.1. In the meantime, the result's noise is also much lower comparing to those with a bigger sdt. Similarly, optimal parameter sets are selected for all three mother wavelets under this situation. It is worth noting that for the DOG mother wavelet, $sdt = 0.9$ is selected as the final choice, sacrificing some smoothness in the result to ensure that the estimated stiffness reaches a value of 150.

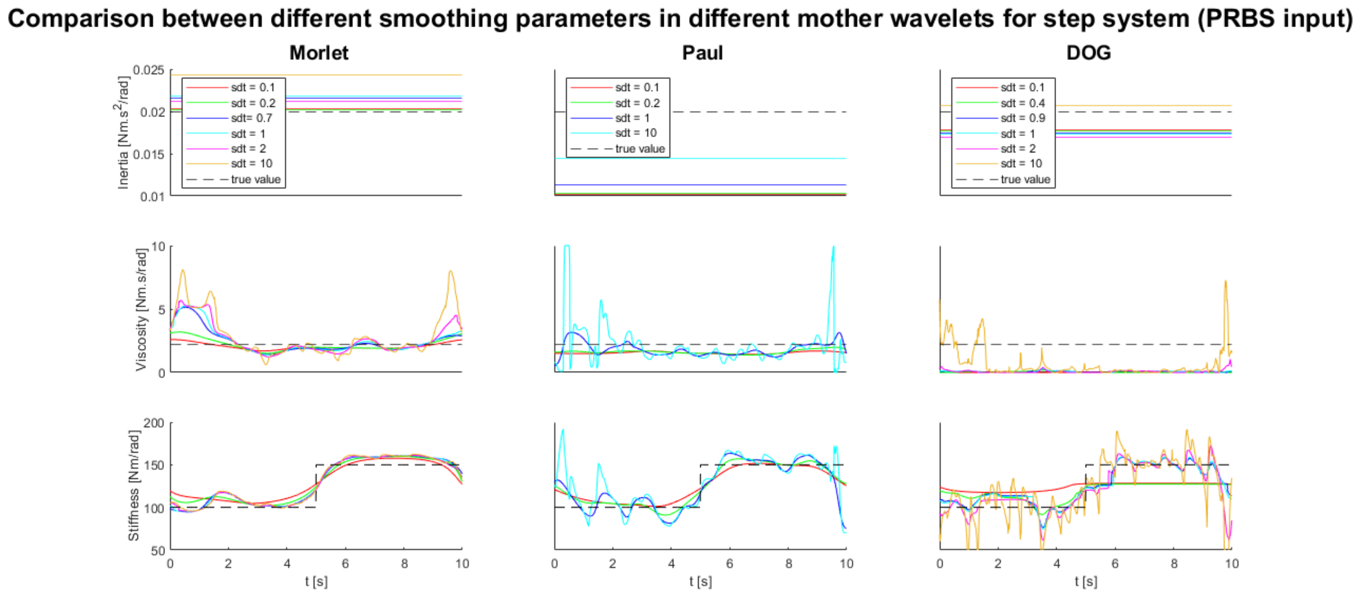

Fig. 15. The estimated result of the parameter selected in Fig. 14 when setting sdj to 0.1. The system to be identified is the step system with a PRBS as input perturbation. Based on these two plots, optimal parameter sets can be chosen for different scenarios.

The same preliminary simulation is performed for all the different scenarios investigated in this study. The results of the performance metrics and estimated time series for each scenarios are included in the Appendix. From these plots, it can be seen that when sdt is larger than 1, there will be only slight difference between results with varying sdt for the Morlet wavelet, the estimated is still rather smooth even that sdt is set to 10. While the result of Paul will be mainly influenced by the sdt on noise, and slightly on the estimated value. And the reuslt of DOG will be influenced both greatly on either the estimated value or noise. Based on these simulations, it can be seen that with a smaller sdt, the estimated result is more smoothing but can barely detect the waveform, corresponding to a higher RMSE and MAE and lower SD. With a higher sdt, the estimated result can better detect the waveform reaching to the lowest and highest value, but the result is usually with a higher noise, which means a lower RMSE and MAE but a higher SD in performance metrics. With all these results, the parameter sets chosen in this study for all the different scenarios are listed in Table .II. The analyzing results in next section is based on these parameter sets.

V. Simulation Result

Using the modified approach and fine-tuned optimal parameters discussed in the last section, the simulation experiment successfully estimate the system identification results for various systems illustrated in Fig. 5. In this section, the results obtained from system identification will be presented and discussed. The results will be categorized and grouped according to the different systems, combining with both PRBS input and filtered noise input. The estimation results obtained using different mother wavelets will be evaluated using various ways, including the performance metrics mentioned earlier, noise levels in the results, accuracy in reaching the exact values, and other relevant criteria. These evaluations will provide a comprehensive analysis of the performance for each mother wavelets in different systems.

A. Step waveform

The non-periodic step function waveform is considered the easiest to identify, and the analysis will start with focusing on this waveform. First, using the estimated inertia, viscosity and stiffness, the estimated torque is successfully calculated as described in Fig. 7. By comparing the estimated torque with the true torque, feasibility of this method is further proven. Both of the estimated torque results for two input perturbations with various mother wavelets are separately shown in Fig. 16 and Fig. 17.

From the analysis of these two plots, it is evident that the system identification method manage to reproduce the torque. The plots show great similarities between the estimated torque and true torque, especially for the system with filtered noise input. The estimated torques for system with PRBS input accurately reproduce the square portions of the waveform. However, it is worth noting that the peaks parts in the estimated torque may appear failed to reproduce the exact value. The Morlet mother wavelets seems to over estimate the value for these peaks. The DOG mother wavelets exhibit the worst performance among the tested wavelets, where seems to be no peaks at all in the estimated result. Regardless of the shortcomings in performance observed among different mother wavelets, the overall results still suggest that this system identification method is still worth further investigation, focusing on either the best mother wavelets for different situation or the optimal parameter sets to reveal the result.

Afterwards, the estimated stiffness results, which is the average across all 100 trials, are plotted for both two different

TABLE II
THE SMOOTHING PARAMETERS USED IN THIS STUDY

		Various Systems														
		Step system			Square system			Sine system			Triangle system			Sawtooth system		
		Morlet	Paul	DOG	Morlet	Paul	DOG	Morlet	Paul	DOG	Morlet	Paul	DOG	Morlet	Paul	DOG
Input PRBS	Smoothing parameter in time sdt	0.2	0.2	0.9	2	2	5	3	2	5	2	2	4	3	5	5
	Smoothing parameter in scale sdj	0.1	0.1	0.1	0.1	0.1	0.1	0.1	0.1	0.2	0.1	0.1	0.1	0.1	0.1	1
Input Filtered noise	Smoothing parameter in time sdt	1	0.3	0.6	2	2	5	2	2	5	10	2	3	2	2	3
	Smoothing parameter in scale sdj	0.1	0.1	0.1	0.1	0.2	0.2	0.1	0.2	0.2	0.1	0.1	0.1	0.1	0.1	0.1

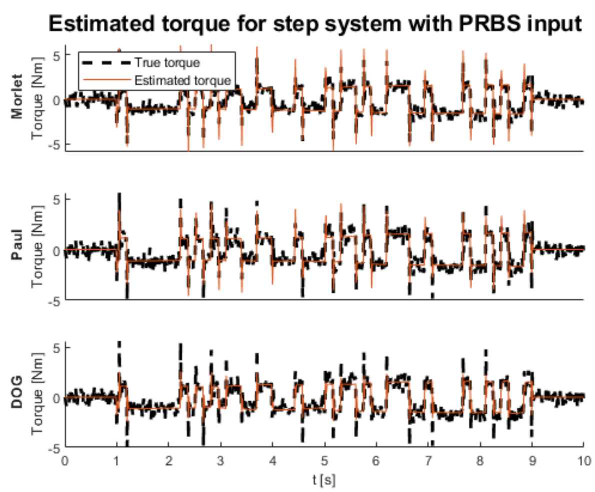

Fig. 16. Comparison between the true torque and estimated torque for step system with PRBS input using different mother wavelets in the system identification method, with orange line indicating the estimated torque and black thick line indicating the true torque. The results further prove the feasibility of the method investigated in this study.

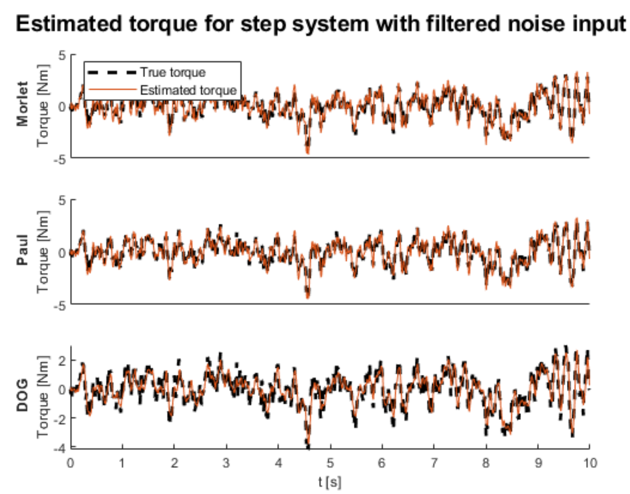

Fig. 17. Comparison between the true torque and estimated torque for step system with filtered noise input using different mother wavelets in the system identification method, with orange line indicating the estimated torque and black thick line indicating the true torque. The results further prove the feasibility of the method investigated in this study.

input perturbations using all three mother wavelets, which is shown in Fig. 18. And the lower plots show the standard deviation (SD) of the average estimated result comparing to the true stiffness.

The plots show that the estimated stiffness mainly reproduce the true stiffness given in the system. In the result of Morlet, the estimated stiffness values in the simulation study successfully reach the exact values of the true system, that is the 50 Nm/rad and 150 Nm/rad. Moreover, the estimated result seems to have the smoothest one among all the three mother wavelets. Specifically, it is observed that the boundary effect has minimal influence on the estimated results for the system with filtered noise as the input perturbation. Regarding the outcome of the Paul wavelet, the estimated value closely approximates the true value. It is worth noting that the rise time appears to be the shortest compared to the other two mother wavelets. The estimated result rapidly rises from 50 Nm/rad to 150 Nm/rad in a brief period, validating the earlier assumptions about the Paul wavelet's superior time localization. Regarding the result of the DOG, despite sacrificing smoothness in order to achieve the closest value to the true stiffness, the outcome remains unsatisfactory. And at the same time the result is quite noisy, which further proves the assumptions made about DOG in previous simulation result. But it is still worth noting that there is a sharp change at the end of rising which better shows the characteristics of sudden change within the true system.

To better show the rise time needed between stages for different mother wavelets, the average derivative of estimated stiffness among all 100 trials is shown in Fig. 19. Only time interval from 5 to 6s has been paid more attention to in this plot. The results of DOG wavelet yields higher peaks compared to the other two wavelets with PRBS input, while the Paul has the highest peak with filtered noise input. However, the result of DOG wavelet is rather noisy, even after the result has been averaged. This phenomenon can be attributed to the presence of noisy, small square-like variations within the estimated stiffness, which corresponds to the split blocks in Fig. 3. When only considering the other two mother wavelets, it appears that Morlet exhibits a higher derivative

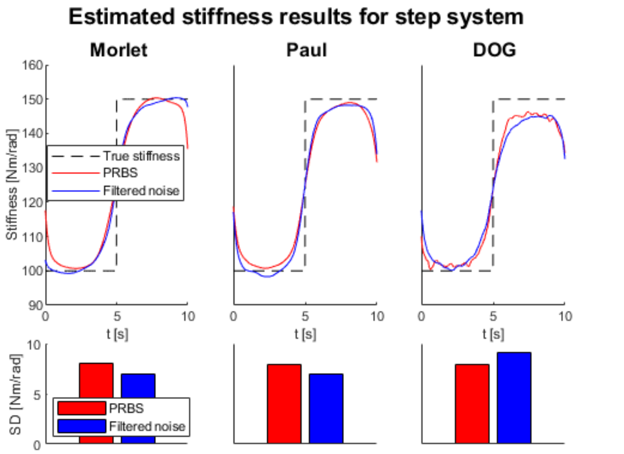

Fig. 18. The three upper plots show the average estimated stiffness results of 100 trials for step system with two different input perturbation using all three mother wavelets, where the dashed lines stand for the true stiffness, the red lines stand for the result of system with PRBS input and blue lines for filtered noise input. From left to right the plot is separately the result of using Morlet, Paul and DOG mother wavelet. The three lower plots show the standard deviation of the average estimated result comparing to the true stiffness, where red bar indicates the PRBS input and blue bar indicates the filtered noise input. The value is separately 7.99, 6.94, 7.93, 6.94, 7.89, 9.07 Nm/rad.

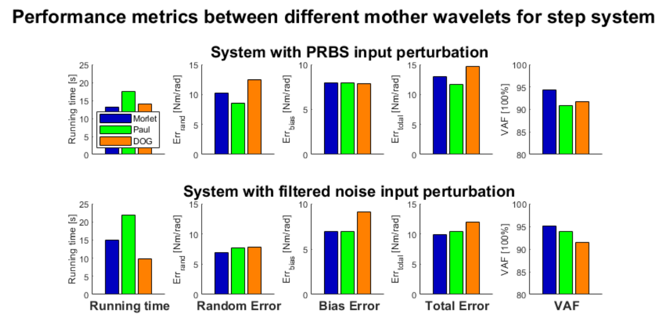

Fig. 20. Performance metrics between different mother wavelets for step system with both PRBS and filtered noise input perturbations. The first row is for the PRBS input and the second row is for the filtered noise. Each column shows a single performance metric. Bars with the same color is the system identification method with different mother wavelets. VAF here is calculated comparing with the noiseless torque.

within a brief period after 5 s. However, Paul quickly surpasses Morlet with a higher value, this well explains the shorter rise time of the estimated stiffness using Paul mother wavelets, which indicates a quicker response of the sharp changing in true system.

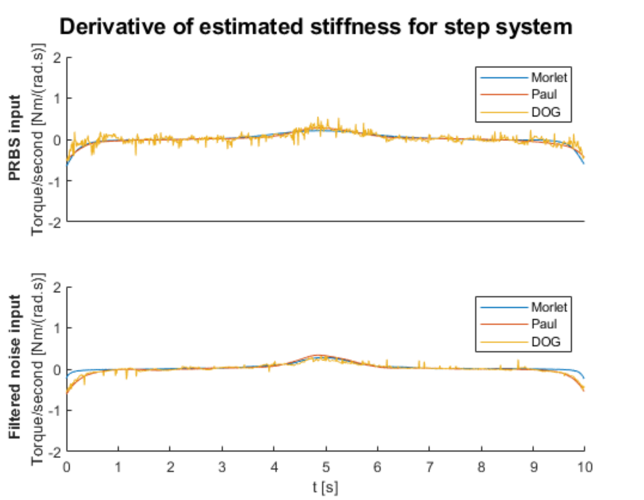

Fig. 19. Average derivatives of estimated stiffness for step system with both input perturbations. The upper plot is for the system with PRBS input and the lower plot is for the system with filtered noise input.

To better compare the difference between different mother wavelets, Fig. 20 presents the performance metrics for all mother wavelets using PRBS and filtered noise as input perturbations.

Regarding the running time, the Paul wavelet is observed to have the longest duration for both input perturbations. Additionally, it can be concluded that the DOG wavelet is more affected by the input type compared to Morlet. Concerning the random error in relation to the true stiffness, the DOG wavelet demonstrates a higher sensitivity to noise, evident from its larger random error. Meanwhile, the Paul wavelet exhibits robustness to input perturbations and displays a lower sensitivity to noise. As to the bias error, it can be concluded that with a filtered noise input, the Morlet and Paul yield better results, which is also what can be seen in Fig. 18. In converse, DOG exhibits a larger bias with filtered noise input due to its not able to reach to the exact value of true stiffness and larger influence brought by boundary effect. Considering the total error combining the randomness and systematic error, Paul wavelet exhibits good performance for both input perturbations. It is noteworthy that when the input perturbation is filtered noise, the Morlet wavelet exhibits the best total error, primarily because it is merely not affected by boundary effects. However, when examining the total error plot of the estimated stiffness, it is expected that the Paul wavelet would exhibit a large variance accounted for, which is in the contrary to the actual result, especially when the input perturbation is PRBS. Morlet wavelet, demonstrates a relatively high VAF, aligning with expectations. Therefore, it can be inferred that the estimated inertia and viscosity for the Paul wavelet may not be satisfactory, contributing to its lower VAF. To further prove this assumption, the estimated inertia and viscosity results for both three mother wavelets are plotted in Fig. 21.

From the plots, it can be seen that the estimated viscosity of the Paul wavelet approximates closer to the true viscosity value comparing with that of DOG wavelet with PRBS as input perturbation, while the estimated inertia deviates from the true inertia compared with other two mother wavelets. This difference could be exactly the reason behind the unexpectedly lower VAF for Paul wavelet with PRBS as input perturbation. It is worth noting from the plot that the estimated viscosity of the DOG wavelet is greatly lower than the true value, which is unexpected and perform much worse than the other two mother wavelets, approaching zero. Moreover, the Morlet wavelet with PRBS as input has the best estimation of both inertia and

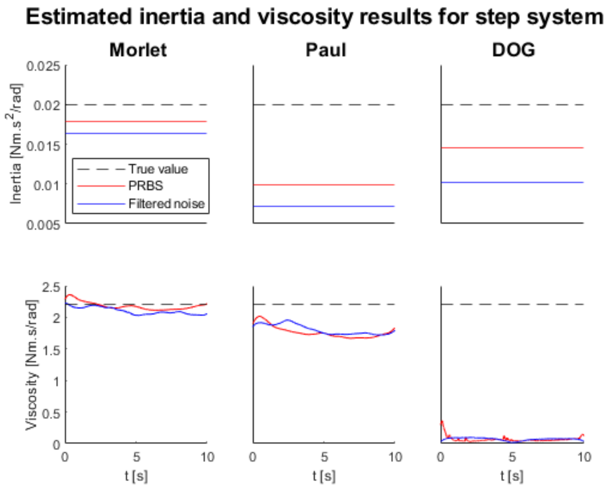

Fig. 21. Estimated inertia and viscosity results for step using different mother wavelets. The upper plots represent estimated inertia and lower parts represent estimated viscosity. The dashed lines stand for the true value in the system.

viscosity.

This part serves as an short example of analyzing the simulation result for various waveforms of system. In the following parts of this section, simulation results will be presented similarly with this part. For all the other systems, only plots with estimated inertia, estimated viscosity, estimated stiffness and performance metrics will be presented.

B. Square waveform

The estimated result across all 40 seconds for the square system is shown in Fig. 22.

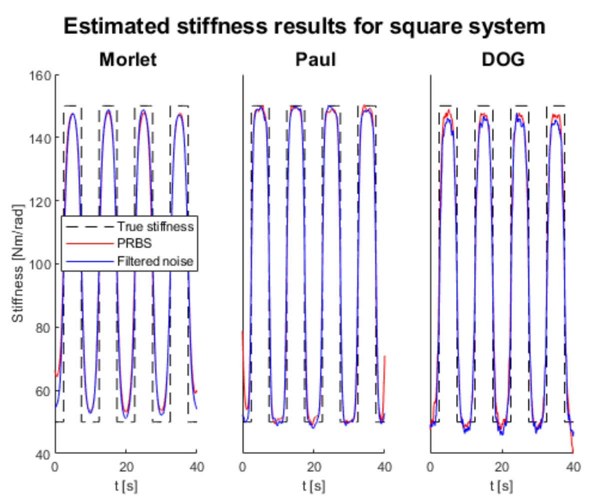

Fig. 22. The average estimated stiffness results across all 40 seconds of simulations for square system in all 6 scenarios.

It can be seen from the figure that the estimated result of Morlet is quite similar to a sine wave. To be mentioned, there is the largest influence brought by the boundary effect when the input perturbation is set to PRBS, while there are almost no boundary effect when setting filtered noise as input. The estimated result of Paul wavelet exhibits the closest shape to a square wave. In the meantime, the result also closely reproduces the true stiffness value. And there are only slight influence brought by boundary effect. As to the DOG's estimated result, the signal seems to undergo a translation in negative y direction. The lower value is smaller than 50 Nm/rad, while the higher value exceeds 150 Nm/rad. Moreover, there exhibits significant noise in areas where a fixed value is expected. But it is worth noting that when the perturbation input is set to PRBS, DOG has the smallest influence brought by boundary effect, especially at the beginning of the signal. To better show the estimation result without boundary effect, an average result of three segments is plotted. These segments range from 5 s to 15 s, 15 s to 25 s, and 25 s to 35 s. The corresponding plot can be referred to as Fig. 23.

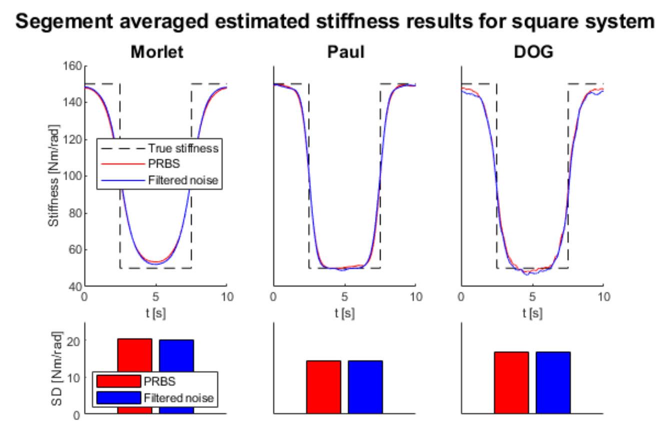

Fig. 23. The average estimated stiffness results of three segments for square system in all 6 scenarios. The standard deviation is separately 20.35, 20.01, 14.47, 14.51, 16.80, 16.93 Nm/rad.

Based on the analysis of this figure, it can be concluded that the Paul wavelet performs better than other wavelets when dealing with a square-shaped system, regardless of the input perturbation. This conclusion is drawn without considering the influence of boundary effects. When excluding the noisy part from consideration, it can be observed that the DOG wavelet also provides a good estimation. To further prove this conclusion, the performance metrics for a square system is shown in Fig. 24.

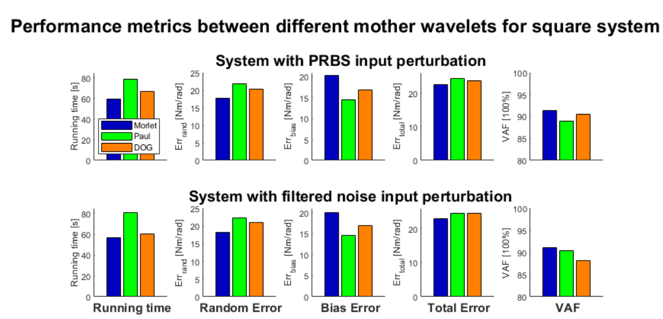

Fig. 24. Performance metrics between different mother wavelets for square system with both PRBS and filtered noise input perturbations.

When dealing with time series with a longer time, the time consumed is rather long for this wavelet based method, with almost 80 s for a single trial when using Paul wavelet. When referring to random error, the Morlet wavelet has the best performance while the Paul wavelet has the worst performance, which means that Paul wavelet is most sensitive to the noise. However, as to the bias error, Paul exhibits the best performance while Morlet has the worst result, which further proves conclusion reached to before. Considering these two error together, the Morlet has the lowest total error for both two kinds of noise. And again, the VAF for Paul wavelet is much lower than expected. Therefore, estimated inertia and viscosity results are shown in Fig. 25.

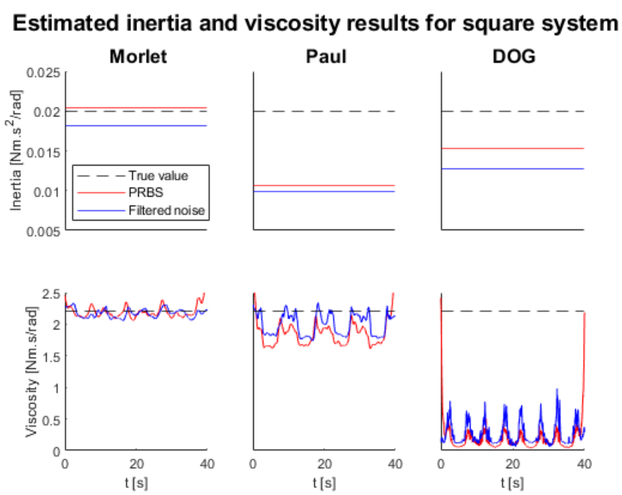

Fig. 25. Estimated inertia and viscosity results for square system using different mother wavelets.

The estimated inertia and viscosity have exactly the same characteristics with the step system. Therefore, low VAF of Paul can be explained by a lower estimated inertia.

The average derivative of estimated stiffness across 100 trials is plotted in Fig. 26. It can be seen that DOG has the maximum value around the time step where there is a sharp change, but the result is rather noisy. The Paul wavelet has the second highest value and a more smooth result.

C. Sine waveform

When the true stiffness is of sine waveform, the estimated result of all 40 seconds is shown in Fig. 27.

Once again, the figure demonstrates that the Paul wavelet consistently gives the best results among all three mother wavelets. This is particularly evident when there is minimal deviation caused by boundary effects, especially when the input perturbation is filtered noise. Furthermore, it can be observed that the estimated result obtained using the DOG wavelet shows negligible boundary effects regardless of the type of input perturbation. The averaged result of one segment is shown in Fig. 28.

The performance metrics for sine system is shown in Fig. 29, where DOG again has the shortest running time and Paul again has the lowest bias error. In the meantime, the Morlet

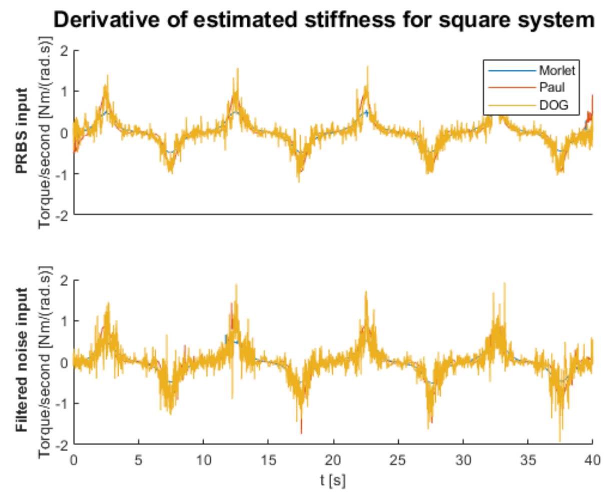

Fig. 26. Average derivatives of estimated stiffness for square system with both input perturbations. The upper plot is for the system with PRBS input and the lower plot is for the system with filtered noise input.

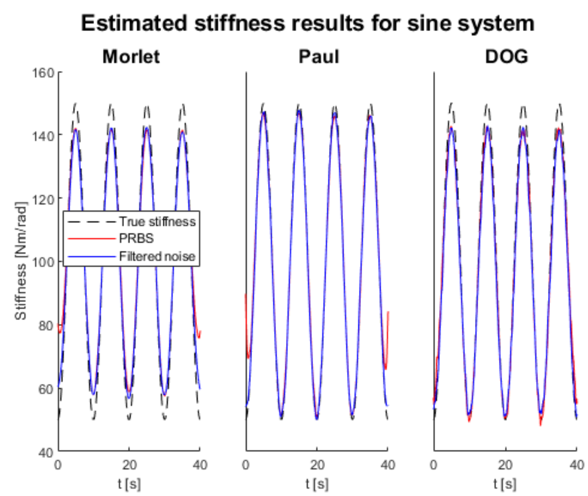

Fig. 27. The average estimated stiffness results across all 40 seconds of simulations for sine system in all 6 scenarios.

wavelet has the lowest random error and total error, also the highest VAF. The performance metrics for sine system has almost same result as the previous square system.

The estimated inertia and viscosity for sine system in shown in Fig. 30, which can serve as an explanation to low VAF for Paul wavelet, where Paul wavelet has a rather low estimated inertia and DOG wavelet has a wrongly estimated viscosity.

The average derivative of estimated stiffness across 100 trials is plotted in Fig. 31. Again result of DOG is much more noisy than the other two mother wavelets and result of Paul has a higher value than that of Morlet around the change of true stiffness.

All these results for sine system seems to have exactly the same conclusion as the square system.

D. Triangle waveform

Fig. 32 displays the estimated result for the entire 40 seconds duration when the true stiffness follows a triangle

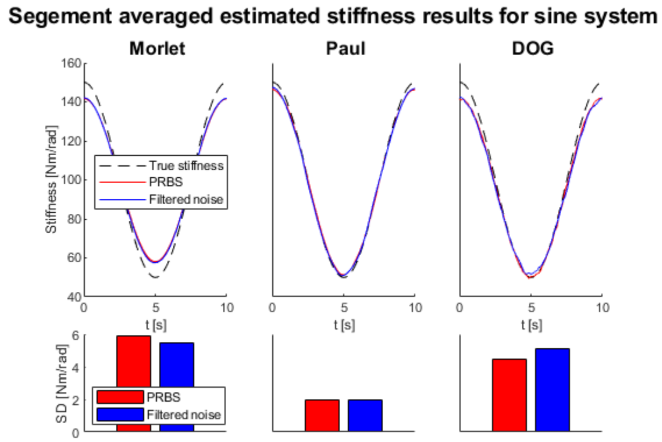

Fig. 28. The average estimated stiffness results of three segments for sine system in all 6 scenarios. The standard deviation is separately 5.89, 5.49, 1.99, 1.93, 4.44, 5.13 Nm/rad.

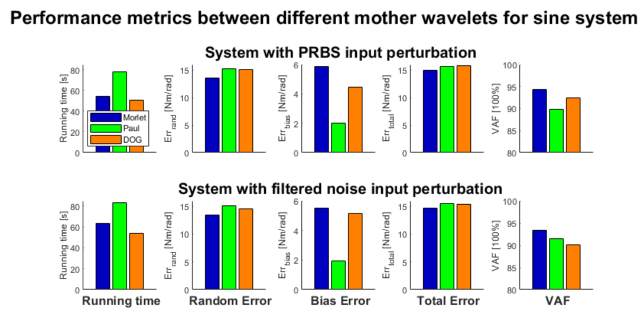

Fig. 29. Performance metrics between different mother wavelets for sine system with both PRBS and filtered noise input perturbations.

waveform.

In this case, none of the mother wavelets successfully imitated the peaks of the triangle waveform, even if the Paul wavelet showing a relatively similar result for the ramp part and a rather close estimation to the true peak value. However, it is worth mentioning that the result of DOG can successfully turn from rising to falling quickly when the other two peaks look more like a circular arc. Similar to the conclusions drawn for the square system, other characteristics related to performance and boundary effects remain consistent. The averaged result in one segment is shown in Fig. 33.

Figure 34 presents the performance metrics for the triangle system across all scenarios.

It can be seen from the plot that again DOG has the shortest running time. And Morlet has the lowest total error and highest VAF. Despite having a relatively small bias error, the total error of the Paul wavelet is the highest among all three mother wavelets. But this error can be reduced by taking average many times, which explains why there is a better approximation in Fig. 33. Compared with the previous performance metrics in both square and step system, that of triangle system has a much better result with lower errors and higher VAFs for all mother wavelets, which shows that this wavelet transform based system identification method is much more suitable

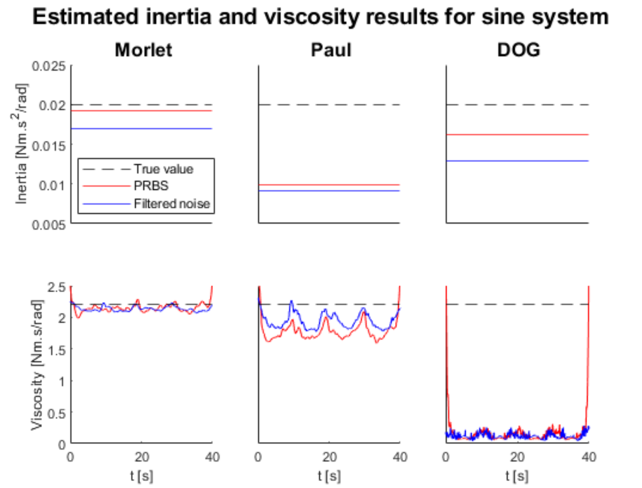

Fig. 30. Estimated inertia and viscosity results for sine system using different mother wavelets.

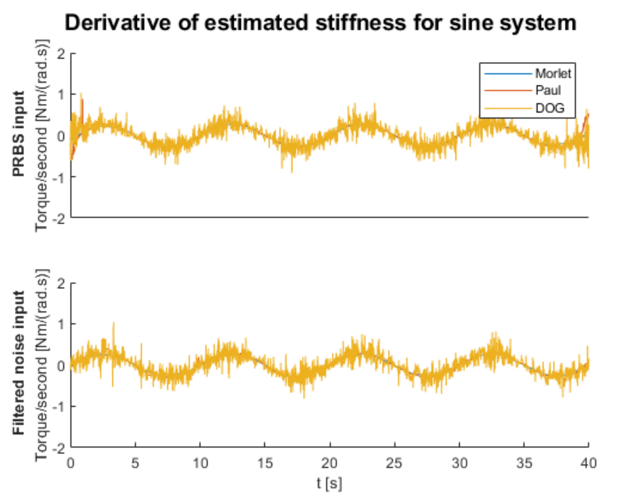

Fig. 31. Average derivatives of estimated stiffness for sine system with both input perturbations. The upper plot is for the system with PRBS input and the lower plot is for the system with filtered noise input.

when dealing with a triangle system.

The estimation results of inertia and viscosity for triangle system is shown in Fig. 35. The estimated result of these two parameters share the same characteristics with all the previous systems.

The rise time is plotted in Fig. 36.

E. Sawtooth waveform

The estimated results for sawtooth system is shown in the Fig. 37.

Similar to the triangle system, none of the three mother wavelets are able to accurately estimate the peak of the waveform. And again Paul wavelet perform best among all three mother wavelets, especially when there is almost no boundary effect with a filtered noise input. From Figure 38, it is evident that only the DOG wavelet detects a sharp change within the estimated result, similar to what was observed in the triangle system. However, Paul and Morlet wavelets have a

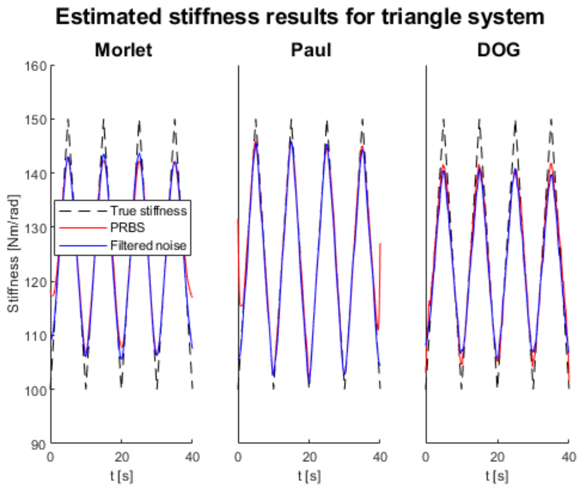

Fig. 32. The average estimated stiffness results across all 40 seconds of simulations for triangle system in all 6 scenarios.

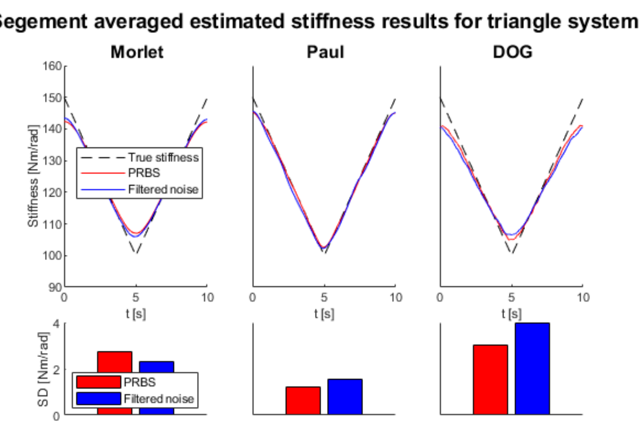

Fig. 33. The average estimated stiffness results of three segments for triangle system in all 6 scenarios. The standard deviation is separately 2.76, 2.29, 1.21, 1.56, 3.04, 3.96 Nm/rad.

better approximation result for the ramp part. The performance metrics for sawtooth system is shown in Fig. 39. Again DOG wavelet has the shortest running time, and Morlet has the lowest total error and highest VAF. In the meantime, Paul wavelet also has the largest random error and the lowest bias error for among all wavelets, same as the conclusion received from the Fig. 38. The rise time is plotted in Fig. 41.

Therefore, to better estimate the sawtooth system when the performing time is not limited and large number of trials are allowed, Paul wavelet would be strongly recommended. If the perturbation input is PRBS and the simulation time is relatively short, the DOG wavelet can be considered as another suitable choice.

VI. Extensions

This section serves as an extension, a supplement explanation to previously encountered interesting problems in this study. This section mainly discusses three topics, effect brought by shorter simulation time on non-periodic waveform,

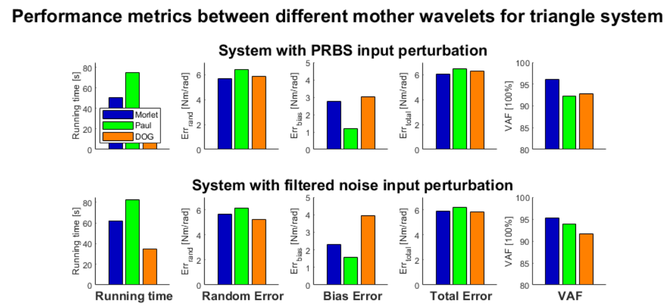

Fig. 34. Performance metrics between different mother wavelets for triangle system with both PRBS and filtered noise input perturbations.

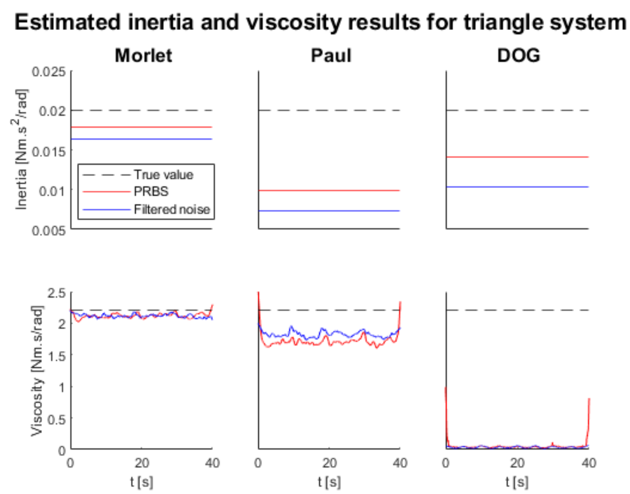

Fig. 35. Estimated inertia and viscosity results for triangle system using different mother wavelets.

longer time on periodic waveforms and also the effect of different SNR. Noticing that all the smoothing parameters used in this part is the same as same scenarios described in Table. II. And it is worth noting that repeating times for a single scenario are lower to 10 to save time.

A. Effect of shorter simulation time on non-periodic waveform

Considering that the previous study focused solely on a duration of 10 seconds for step waveform, an intriguing topic arises when considering non-periodic systems with very short time intervals. In such cases, where boundary effects inevitably impact the estimation results, will the best mother wavelet to be used switch to another one? This part will firstly focus on this topic. The experiment is performed with a simulation time of 3s, and the estimated stiffness results are shown in Fig. 42.

Comparing with the estimated result in Fig. 18, the estimated result is much further from a step waveform, especially when DOG is selected as the mother wavelet used during the method. In the meantime, the standard deviation (SD) is also much higher than that of when the simulation time is 10s. It also can be seen from the figure that the estimated result is greatly affect when choosing PRBS as the input perturbation. To better evaluate the best mother wavelet, performance metrics under this situation is given in Fig. 43 and rise time is shown in Fig. 44.

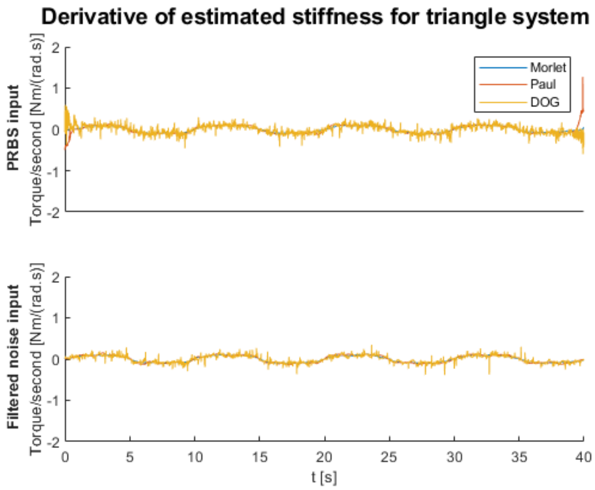

Fig. 36. Average derivatives of estimated stiffness for triangle system with both input perturbations. The upper plot is for the system with PRBS input and the lower plot is for the system with filtered noise input.

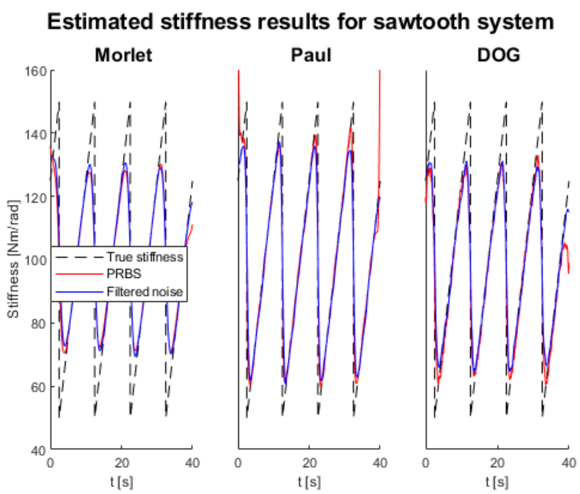

Fig. 37. The average estimated stiffness results across all 40 seconds of simulations for sawtooth system in all 6 scenarios.

When only considering the filtered noise input perturbation with Morlet and Paul mother wavelet, Paul has a better performance given that both a lower bias error and total error even when there is a higher random error. However, Morlet still appears to have a better VAF. Moreover, it can be concluded from the derivative of estimated stiffness that there will be a short delay in rising when using Paul as the mother wavelet under this situation.

B. Effect of longer simulation time on periodic waveforms

In contrast, a longer simulation time for periodic waveform generally improve the performance of parameter estimation [2]. It is also worth trying what is the effect brought by longer simulation time for different mother wavelets, will the best mother wavelet again switch to another one? This is the second topic to be discussed in this section. This topic will be discussed using square system as an example.

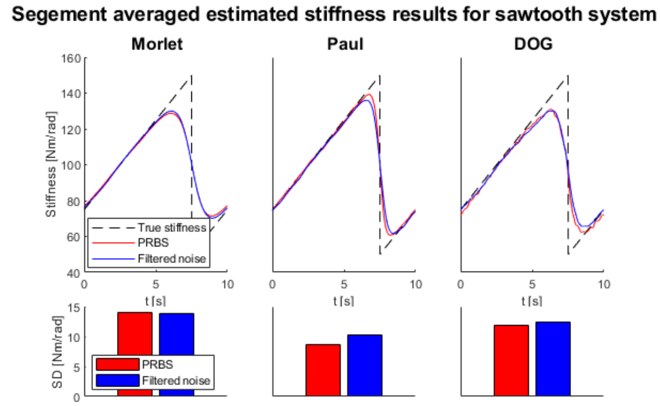

Fig. 38. The average estimated stiffness results of three segments for sawtooth system in all 6 scenarios. The standard deviation is separately 14.08, 13.90, 8.74, 10.34, 11.78, 12.46 Nm/rad.

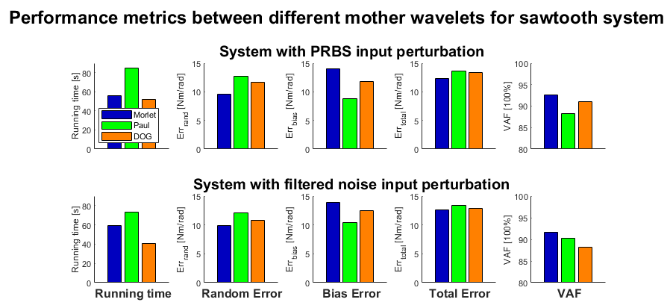

Fig. 39. Performance metrics between different mother wavelets for sawtooth system with both PRBS and filtered noise input perturbations.

To find the effect brought by longer simulation time for periodic waveform, experiments with simulation time of 80, 150, 300 and 600 seconds are performed. The discussions primarily focus on experiments involving PRBS noise. For each simulation duration, the smoothing parameters in both time sdt and scale sdj are re-chosen. All the optimized smoothing parameters in scale sdj are consistently set to 0.1. The roughly selected smoothing parameters in time sdt used are listed in Table III, and the estimated result across segments and performance metrics are separately shown in Fig. 45 and Fig. 46.

Only slight difference can be seen from the estimated result for Morlet and Paul mother wavelets. As to DOG mother wavelet, even if the smoothing parameters haven been roughly optimized, the estimated result seems to become worse when the simulation time is enlarged. For Morlet mother wavelet,

	Morlet	Paul	DOG
T=600s	10	10	20
T=300s	5	10	10
T=150s	5	5	10
T=80s	2	2	5

TABLE III
SMOOTHING PARAMETER IN TIME sdt SELECTED FOR THE EXPERIMENTS WITH LONGER SIMULATION TIME

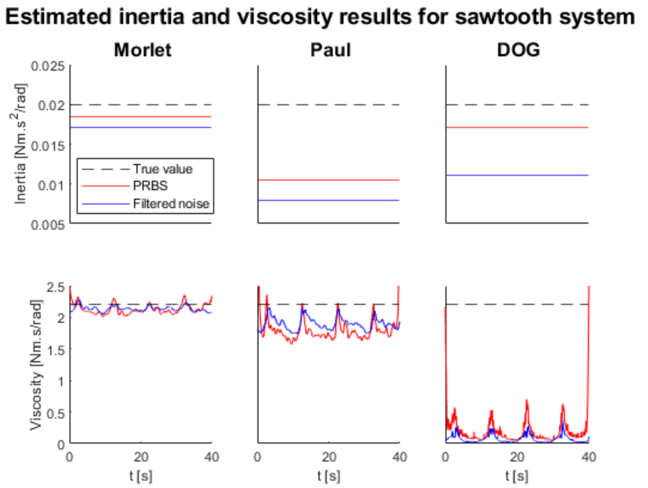

Fig. 40. Estimated inertia and viscosity results for sawtooth system using different mother wavelets.

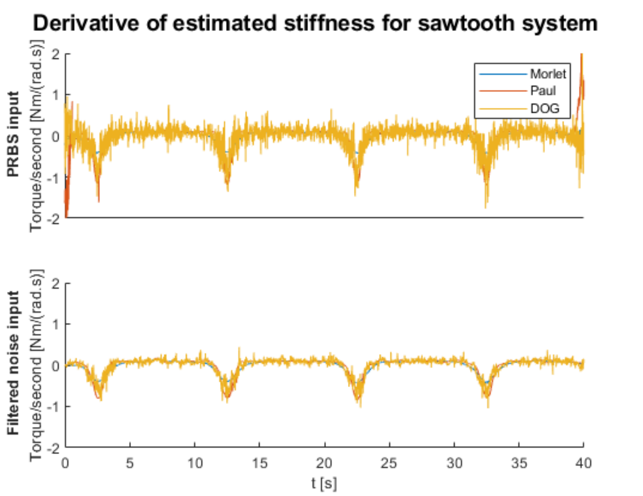

Fig. 41. Average derivatives of estimated stiffness for sawtooth system with both input perturbations. The upper plot is for the system with PRBS input and the lower plot is for the system with filtered noise input.

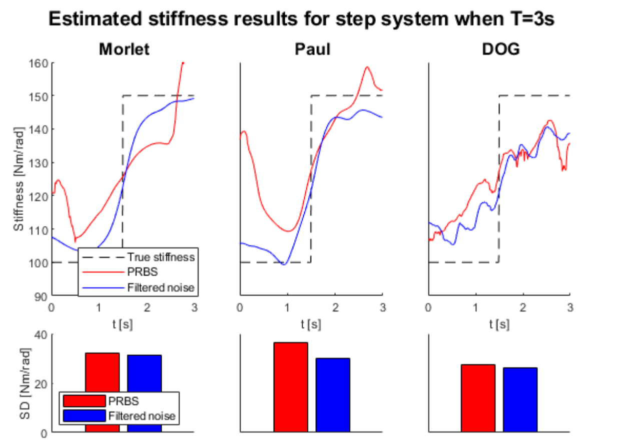

Fig. 42. Estimated stiffness result for step system when simulation time is 3s.

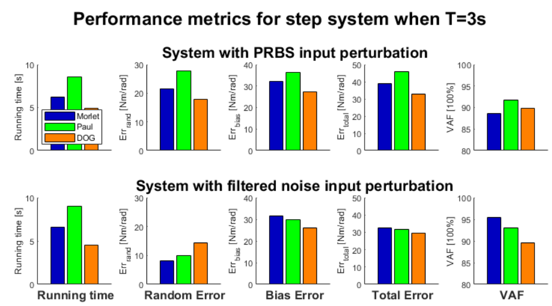

Fig. 43. Performance metrics for step system when simulation time is 3s.

small improvements can be seen when simulation time changes from 300 seconds to 600 seconds, with a larger smoothing parameter in time sdt. This improvement is much more significant for Paul mother wavelet, the estimated result gradually improves from 80 seconds to 300 seconds with an increasing sdt. This strongly proves the necessity of optimizing before applying this system identification method.

Considering the performance metrics, there is indeed a descending trend in random error and total error for all three mother wavelets and also a increasing trend in VAF. However, there is a increasing trend in the bias error for all three mother wavelets. As to comparing the performance between these three mother wavelets, it seems Paul still has the lowest error and Morlet has the highest VAF.

In conclusion, it will be recommended for this system identification method to be applied to the time series where the simulation time is not that long with few repeated times considering both the running time and the error performance.

C. Effect of different SNR

Considering random error of Paul wavelet has a relative high value for both triangle and sawtooth system, which means more sensitive to the noise. Therefore, signal to noise ratio (SNR) is set to different values, separately -10, 0, 10, 20, 30 dB to see the change in performance of three mother wavelets in the square waveform system. The estimated stiffness results are shown in Fig. 47. There is only a slight distinction observed among these estimated results across varying SNR.

The performance metrics for different SNR is shown in Fig. 48. These values remain almost constant for varying SNR, especially for Morlet wavelet. It is worth noting that when SNR is set to 20 dB, the results exhibit a slightly higher error compared to the others when Paul is chosen as the mother wavelet. The conclusion remains consistent with the findings presented in the previous section: Paul has a lower bias error and total error, while Morlet has the lowest random error and the highest VAF. Therefore, it can be concluded that the selection of mother wavelet in this wavelet transform based sysID method will not be affected by SNR.

VII. Discussion

In this study, performance of different mother wavelets in various scenarios has been investigated. Not only systems with various waveforms of stiffness have been tested, but also the system with different kinds of perturbation input. Besides,

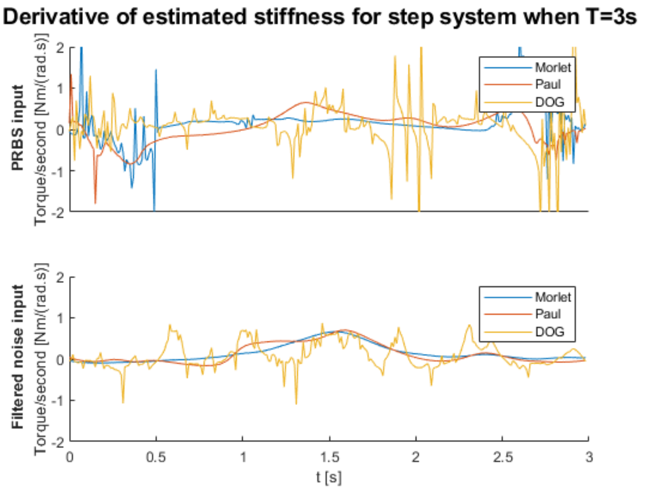

Fig. 44. Derivative of estimated stiffness for step system when simulation time is 3s.

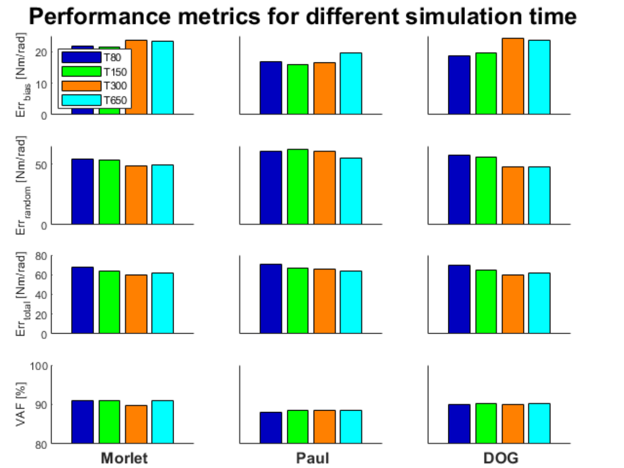

Fig. 46. Performance metrics for square system across varying simulation time.

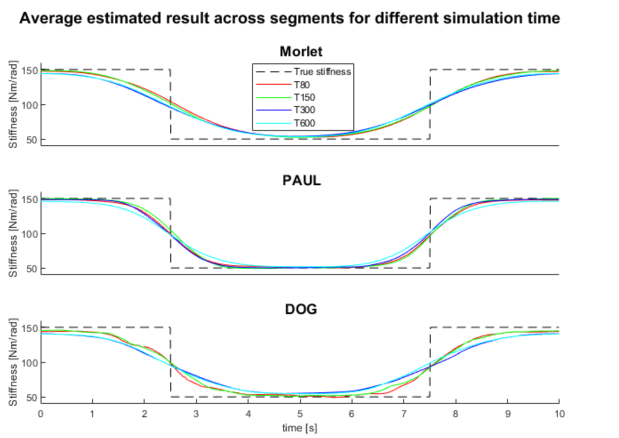

Fig. 45. Estimated stiffness result for square system across varying simulation time.

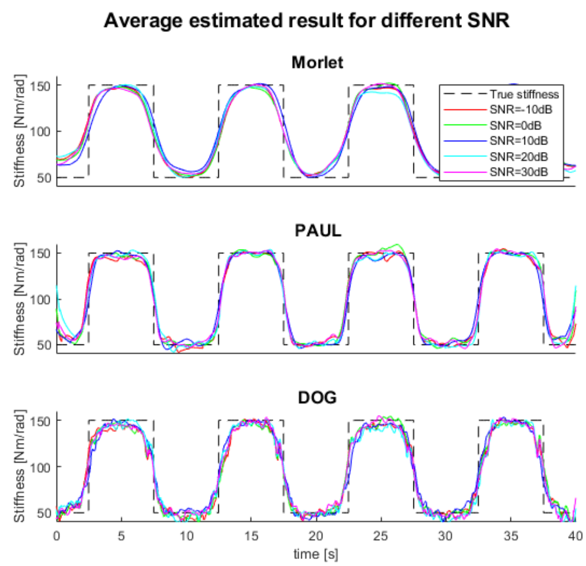

Fig. 47. Estimated stiffness result for square system across varying SNR.

the threshold at which the estimated result more accurately approximates the true stiffness, performance over longer simulation times and performance of torque with higher SNR has also been discussed in this study. The findings of this study can be served as a preliminary simulation and lay the groundwork for further research. Based on these results, a short guidance for using this wavelet based system identification method for a system with time-invariant inertia, viscosity and time-varying stiffness can be given for different scenarios:

1) When the stiffness is non-periodic step function, using Paul mother wavelet yields the most accurate approximation of the jump between two stages if not considering boundary effect. However, the lowest total error and highest VAF will be realized using Morlet wavelet with the filtered noise input. In the meantime, if the total simulation time is too short, for example 3 seconds, then using Morlet wavelet with the filtered noise input to the system will result in the best result.
2) When the stiffness is periodic function, Paul is the mother wavelet can find the closet value comparing to the true stiffness with the lowest SD of averaged result comparing to true stiffness, this is not affected by whatever the periodic waveform is. The large random error in result can be reduced by doing average both across trials and different segments without boundary effect. The highest VAF and lowest random and total error can be received using Morlet wavelet. To be mentioned, if the total simulation time is too short with only 1 or 2 segments and the input perturbation has to be the PRBS input, then DOG is preferred as the mother wavelet.
3) When estimated stiffness is preferred to be as smooth as possible, then Morlet will be the choice.
4) When there is limited time available to obtain the estimation result, such as when fewer trials are allowed for repetition or when time constraints exist for a single trial, the DOG wavelet becomes the preferred choice as the mother wavelet.

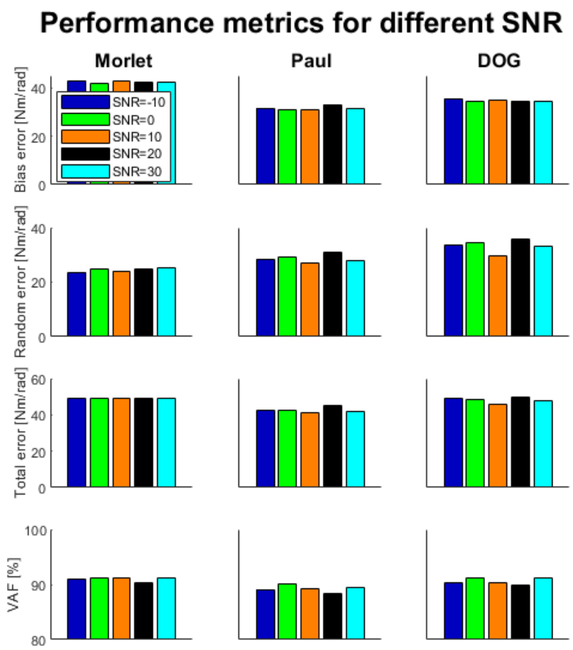

Fig. 48. Performance metrics of different scenarios with varying SNR.

5) When estimated inertia and viscosity is preferred as the final result, then Morlet will be the only choice as mother wavelet.

Certainly, there are still numerous topics for exploration and investigation in future studies based on this method. The following sections will introduce five new topics for discussion, separately exploring other mother wavelets, smoothing function before estimation, optimization of other method parameters exploring systems can be detected, exploring the relation between simulation time and smoothing parameter in time,. These topics open up new directions for future studies, enabling a deeper understanding and potential enhancements of the method studied.

A. Exploring other mother wavelets

Wavelet analysis has been a rapidly developing field, especially in recent years, resulting in the proposal of numerous new wavelet functions. Examples of such wavelets include the Haar wavelet, Daubechies wavelets, Coiflets, and Symlets wavelets. These new wavelets offer different characteristics and properties, offering more options to choose from in different scenarios of signal processing. Ngui's conclusion suggests that the selection of mother wavelets primarily relies on the similarity between the signal and the chosen wavelet [10].

However, this study is mainly based on the wavelet package developed by Torrence, focusing only on three non-orthogonal wavelets, namely Morlet, Paul and DOG. Therefore, we believe that there are still underlying optimal mother wavelets in the field of identifying human joint impedance. Other frequently used mother wavelets in neuromechanics control are suggested to be used as test object in future studies. Examples of such wavelets include Daubechies, Symlet and Mexican hat wavelets [28]. Daubechies and Symlet are well-known examples of orthogonal mother wavelets, which differ significantly from the three mother wavelets used in this study. These two mother wavelets are separately plotting in Fig. 49 and Fig. 50 provided in Wavelet Toolbox in MathWorks. It can be seen these two mother wavelets are with total different shape from the three symmetric mother wavelets used in this study. Moreover, they exhibit a closer shape to the torque time-series being applied, may result in more similar estimation results. It is believed that integrating these two mother wavelets into this system identification method will come to substantially different performance results.

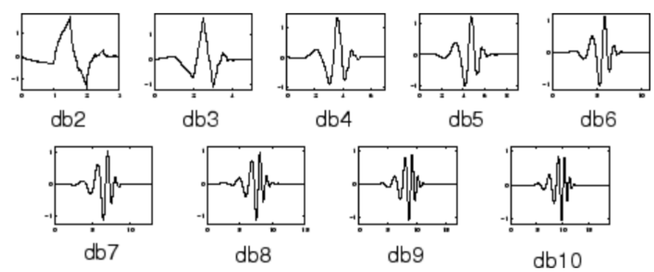

Fig. 49. Shapes of Daubechies wavelet family, where n is the order, and db short for Daubechies. Db1 has the exact same shape as the Haar mother wavelet.

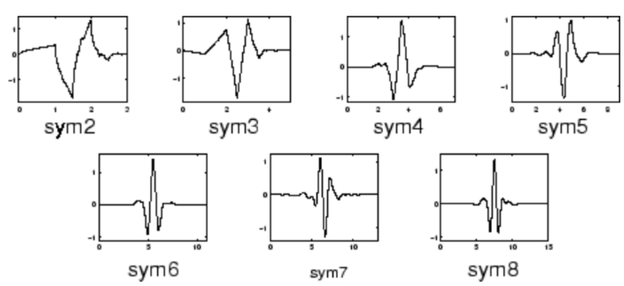

Fig. 50. Shapes of Symlet wavelet family, where n is the order, and sym short for Symlet. The properties of the two wavelet families are similar.

B. Smoothing function before estimation

As discussed in Section 2, the Gauss function and boxcar function is separately used for smoothing in times and in scale. These two smoothing method is proposed by Torrence [8]. However, the paper mentions other smoothing methods as well, such as using damped cosine or white noise. The two used in this study are just brief examples discussed by Torrence. Additionally, it is worth noting that the smoothing operator tends to have improved performance when its shape closely matches that of the mother wavelets. This suggests that there may be other more suitable smoothing operators that can be explored for better results in different mother wavelets, noticing that all three mother wavelets share the same smoothing operators in this study.

C. Optimization of other parameters

In this study, only the influence of the smoothing parameters and initial points of the least square method on the final results have been tested and discussed. However, there are still lots of parameters to be extensively discussed or investigated to optimum the estimation performance for different mother wavelets. The most interesting parameter is definitely the parameter within mother wavelets itself, the k within Eq. 5, 6 and 7. In this study, all the simulation is based on setting k to 6, 4 and 6 separately for Morlet, Paul and DOG wavelets. As mentioned by Moortel, this value also greatly affect the characteristics of these mother wavelets [9]. This can be seen in Fig. 51 and Fig. 52, which is plotted with the same data to be applied with CWT while changing value of k.

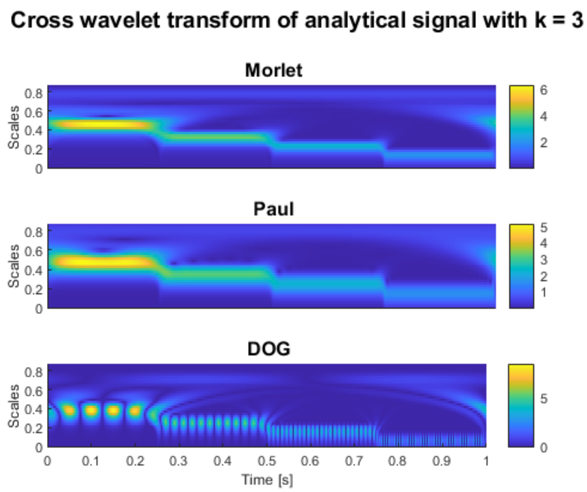

Fig. 51. CWT result of the analytical signal used in Moortel's paper with $k = 3$, slight differences can be seen comparing to Fig. 3.

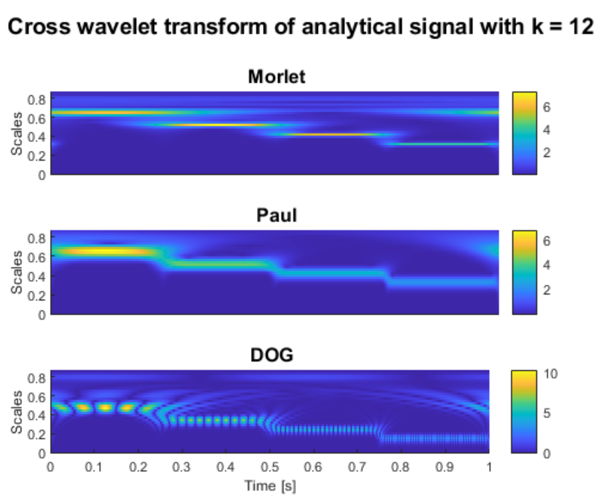

Fig. 52. CWT result of the analytical signal used in Moortel's paper with $k = 12$, great differences can be seen comparing to Fig. 51.

The results indicate that when the value of k is set to a larger value, the characteristic of the mother wavelets become more evident. However, this also leads to more prominent shortcomings associated with each wavelet. Therefore, in order to fully make use of the advantages offered by each mother wavelet and avoid the prominent shortcomings, it is necessary to find a specific order that optimizes their respective strengths.

Besides, there are also lots of other parameters used in the wavelet transform, for example the smallest scale $S0$, the spacing between discrete scales DJ. These may all have influence on the final estimation result.

D. Exploring systems can be detected

During the experiment, it has been proved that no matter what mother wavelets to be used and the values assigned to the smoothing parameters, the wavelet-based method cannot be effectively applied to a system with a stiffness frequency of 0.5 Hz while keeping all other values fixed, to achieve accurate approximation of results. An example estimated result is given in Fig. 53. It can be seen from the figure that even if the estimated torque is almost accurately reproduced, the estimated result of stiffness is rather noisy for all three mother wavelets. Therefore, it can be inferred that there exists a threshold in the relationship between the amplitude and frequency of stiffness, beyond which the wavelet-based method accurately identify the results. It will be worth trying to find this threshold for the system to be identified.

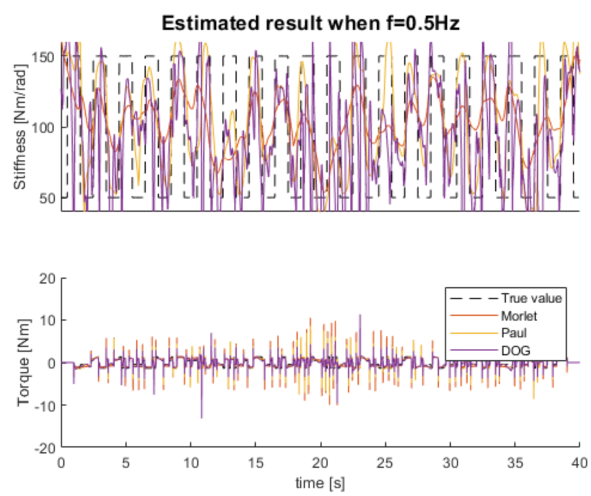

Fig. 53. Example estimated result of the system with a stiffness frequency of 0.5 Hz.

E. Exploring the relation between simulation time and smoothing parameter in time

Described by Section 4.B, when the simulation time is enlarged there should also be a increasing in smoothing parameter in time sdt to ensure the accuracy of the estimated result. Therefore, it will be also interesting to find this relationship between the optimized smoothing parameter in time and the simulation time.

VIII. Conclusion

The wavelet-based method has been proved to be a rather effective way to identify the human joint impedance. However, there are lots to consider when referring to wavelet analysis. Considering that there are different mother wavelets with various characteristics, it becomes obvious that specific scenarios may arise where a particular mother wavelet is the most suitable choice. This study investigates the performance of three mother wavelets in different scenarios. The findings from this investigation can provide valuable insights and serve as a guideline for further research in the field. Additionally, this study offers some additional guidance for extending the application of this wavelet-based method in future studies. As a result, future studies can use these guidance to select the most appropriate mother wavelets for their specific research needs.

IX. Acknowlegement

I express my gratitude to my daily supervisor Mark for providing valuable comments and guidance throughout my work. Additionally, I extend my appreciation to Professor Alfred, who introduced me to the fascinating field of system identification and parameter estimation through the course "System Identification and Parameter Estimation". I find it particularly interesting to conduct experiments involving time series signals in both the time and frequency domains. It allows for fascinating explorations and insights into the properties and transformations of the data.

References

[1] J. D. Hamilton, *Time series analysis*. Princeton university press, 2020.
[2] M. van de Ruit, W. Mugge, G. Cavallo, J. Lataire, D. Ludvig, and A. C. Schouten, "Quantitative comparison of time-varying system identification methods to describe human joint impedance," *Annual reviews in control*, vol. 52, pp. 91–107, 2021.
[3] R. E. Kearney and I. W. Hunter, "System identification of human joint dynamics." *Critical reviews in biomedical engineering*, vol. 18, no. 1, pp. 55–87, 1990.
[4] Y.-F. Sang, D. Wang, J.-C. Wu, Q.-P. Zhu, and L. Wang, "The relation between periods' identification and noises in hydrologic series data," *Journal of Hydrology*, vol. 368, no. 1-4, pp. 165–177, 2009.
[5] D. Ludvig and E. J. Perreault, "System identification of physiological systems using short data segments," *IEEE transactions on biomedical engineering*, vol. 59, no. 12, pp. 3541–3549, 2012.
[6] K. J. Åström and P. Eykhoff, "System identification—a survey," *Automatica*, vol. 7, no. 2, pp. 123–162, 1971.
[7] A. C. S. David Balderas and E. de Vlugt, "Time-varying identification of human properties using the wavelet analysis," Master's Thesis.
[8] C. Torrence and G. P. Compo, "A practical guide to wavelet analysis," *Bulletin of the American Meteorological society*, vol. 79, no. 1, pp. 61–78, 1998.
[9] I. De Moortel, S. Munday, and A. W. Hood, "Wavelet analysis: the effect of varying basic wavelet parameters," *Solar Physics*, vol. 222, no. 2, pp. 203–228, 2004.
[10] W. K. Ngui, M. S. Leong, L. M. Hee, and A. M. Abdelrhman, "Wavelet analysis: mother wavelet selection methods," *Applied mechanics and materials*, vol. 393, pp. 953–958, 2013.
[11] A. N. Akansu and R. A. Haddad, *Multiresolution signal decomposition: transforms, subbands, and wavelets*. Academic press, 2001.
[12] F. Jurado and J. R. Saenz, "Comparison between discrete stft and wavelets for the analysis of power quality events," *Electric power systems research*, vol. 62, no. 3, pp. 183–190, 2002.
[13] wiki, "wavelet wiki," https://en.wikipedia.org/wiki/Wavelet#Mother_wavelet.
[14] Y.-F. Sang, V. P. Singh, F. Sun, Y. Chen, Y. Liu, and M. Yang, "Wavelet-based hydrological time series forecasting," *Journal of Hydrologic Engineering*, vol. 21, no. 5, p. 06016001, 2016.
[15] C. Torrence and P. J. Webster, "Interdecadal changes in the enso–monsoon system," *Journal of climate*, vol. 12, no. 8, pp. 2679–2690, 1999.
[16] R. F. Kirsch and R. E. Kearney, "Identification of time-varying stiffness dynamics of the human ankle joint during an imposed movement," *Experimental brain research*, vol. 114, pp. 71–85, 1997.
[17] D. Ludvig, T. S. Visser, H. Giesbrecht, and R. E. Kearney, "Identification of time-varying intrinsic and reflex joint stiffness," *IEEE transactions on biomedical engineering*, vol. 58, no. 6, pp. 1715–1723, 2011.
[18] D. Crecraft and D. Gorham, *Electronics*. CRC Press, 2002.
[19] Y. Wei and Q. Zhang, *Common Waveform Analysis: a new and practical generalization of Fourier analysis*. Springer Science & Business Media, 2012, vol. 9.
[20] D. L. Guarin and R. E. Kearney, "Unbiased estimation of human joint intrinsic mechanical properties during movement," *Ieee Transactions on Neural Systems and Rehabilitation Engineering*, vol. 26, no. 10, pp. 1975–1984, 2018.
[21] M. L. Johnson and L. M. Faunt, "[1] parameter estimation by least-squares methods," in *Methods in enzymology*. Elsevier, 1992, vol. 210, pp. 1–37.
[22] K. Park and P. H. Chang, "Stochastic estimation of human shoulder impedance with robots: An experimental design," in *2011 IEEE International Conference on Rehabilitation Robotics*. IEEE, 2011, pp. 1–8.
[23] E. J. Perreault, R. F. Kirsch, and A. M. Acosta, "Multiple-input, multiple-output system identification for characterization of limb stiffness dynamics," *Biological cybernetics*, vol. 80, no. 5, pp. 327–337, 1999.
[24] T. Chai and R. R. Draxler, "Root mean square error (rmse) or mean absolute error (mae)," *Geoscientific model development discussions*, vol. 7, no. 1, pp. 1525–1534, 2014.
[25] C. J. Willmott and K. Matsuura, "Advantages of the mean absolute error (mae) over the root mean square error (rmse) in assessing average model performance," *Climate research*, vol. 30, no. 1, pp. 79–82, 2005.
[26] D. K. Lee, J. In, and S. Lee, "Standard deviation and standard error of the mean," *Korean journal of anesthesiology*, vol. 68, no. 3, pp. 220–223, 2015.
[27] H. Su, Q. Liu, and J. Li, "Boundary effects reduction in wavelet transform for time-frequency analysis," *Wseas transactions on signal processing*, vol. 8, no. 4, pp. 169–179, 2012.
[28] P. S. Addison, "Wavelet transforms and the ecg: a review," *Physiological measurement*, vol. 26, no. 5, p. R155, 2005.

Appendix

Abbreviations

The following is the abbreviations for the commonly used words in this report:

TS	Time Series
WT	Wavelet Transform
sysID	System Identification
STFT	Short-time Fourier Transform
XWT	Cross-Wavelet Transform
DOG	Derivate of Gaussian
CWT	Continuous Wavelet Transform
FRF	Frequency Response Function
PRBS	Pseudo Random Binary Sequence
SNR	Signal to Noise Ratio
VAF	Variance-accounted-for
RMSE	Root Mean Square Error
MAE	Mean Absolute Error
SD	Standard Deviation

Comparison for different parameters

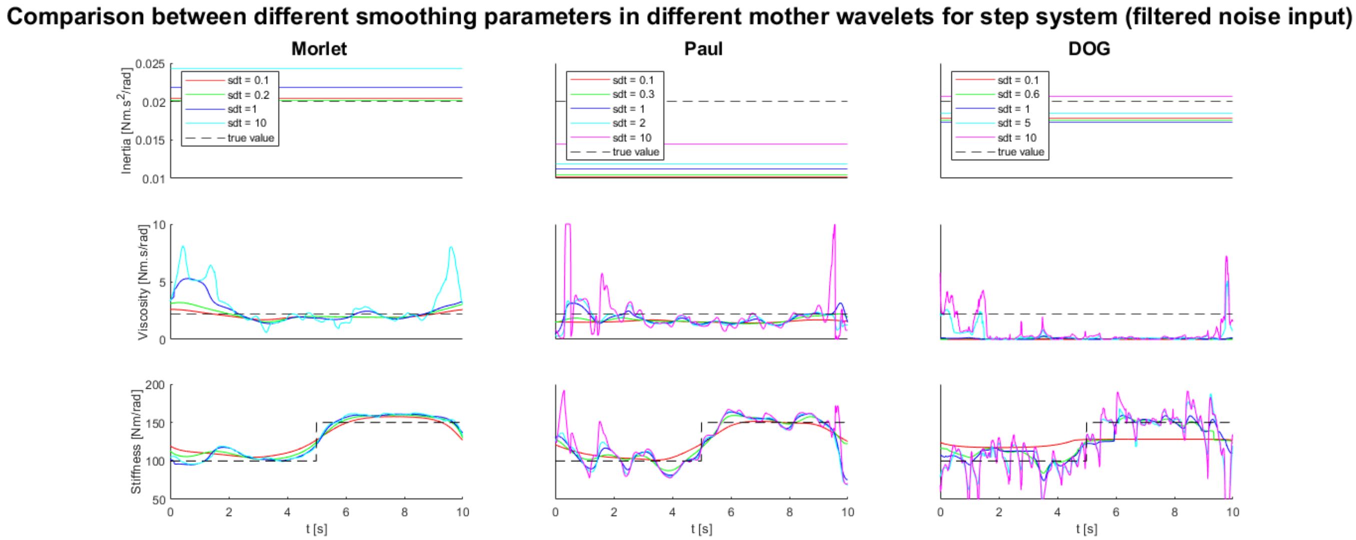

Fig. 54. The estimated result of the parameters selected. The system to be identified is the step system with a filtered noise as input perturbation.

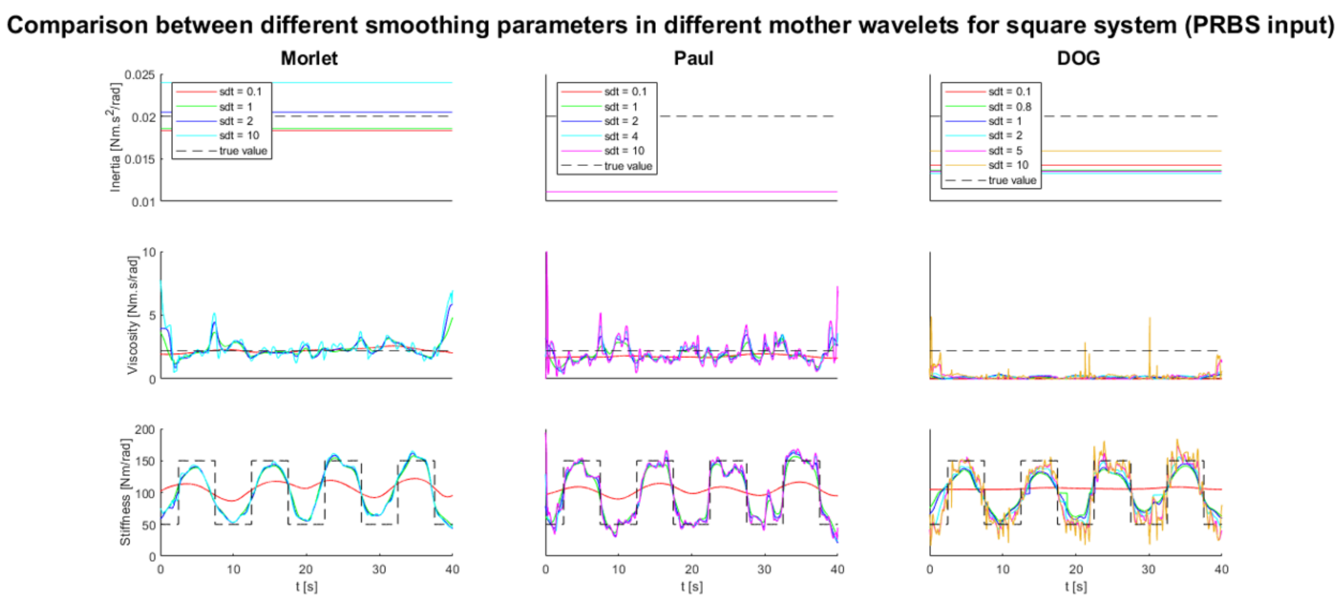

Fig. 55. The estimated result of the parameters selected. The system to be identified is the square system with a PRBS as input perturbation.

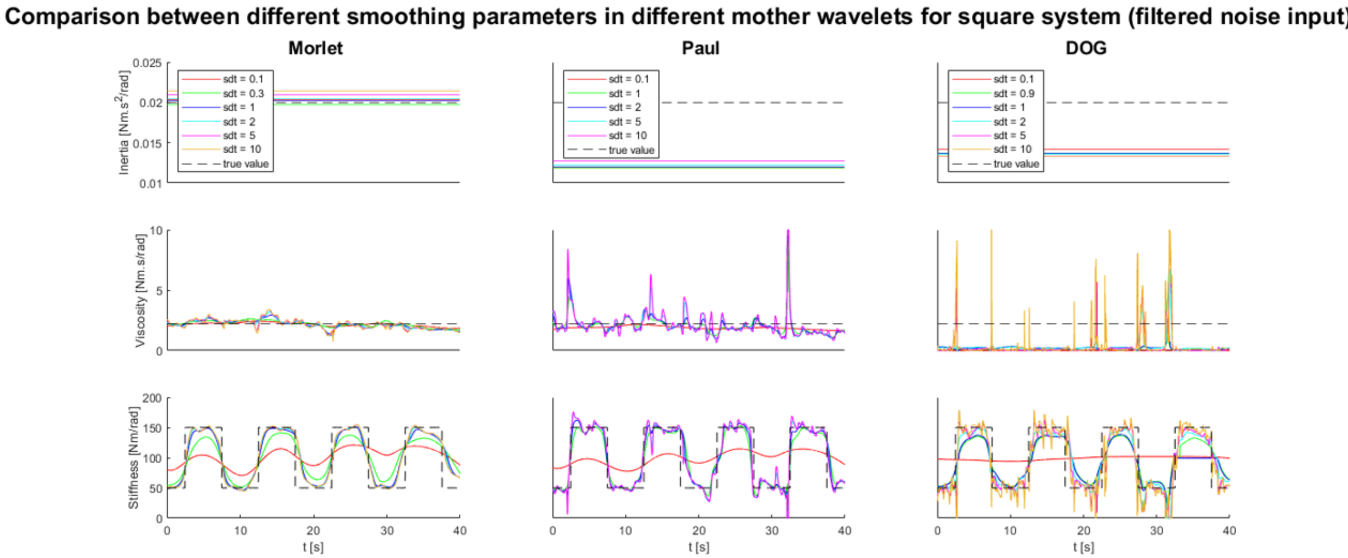

Fig. 56. The estimated result of the parameters selected. The system to be identified is the square system with a filtered noise as input perturbation.

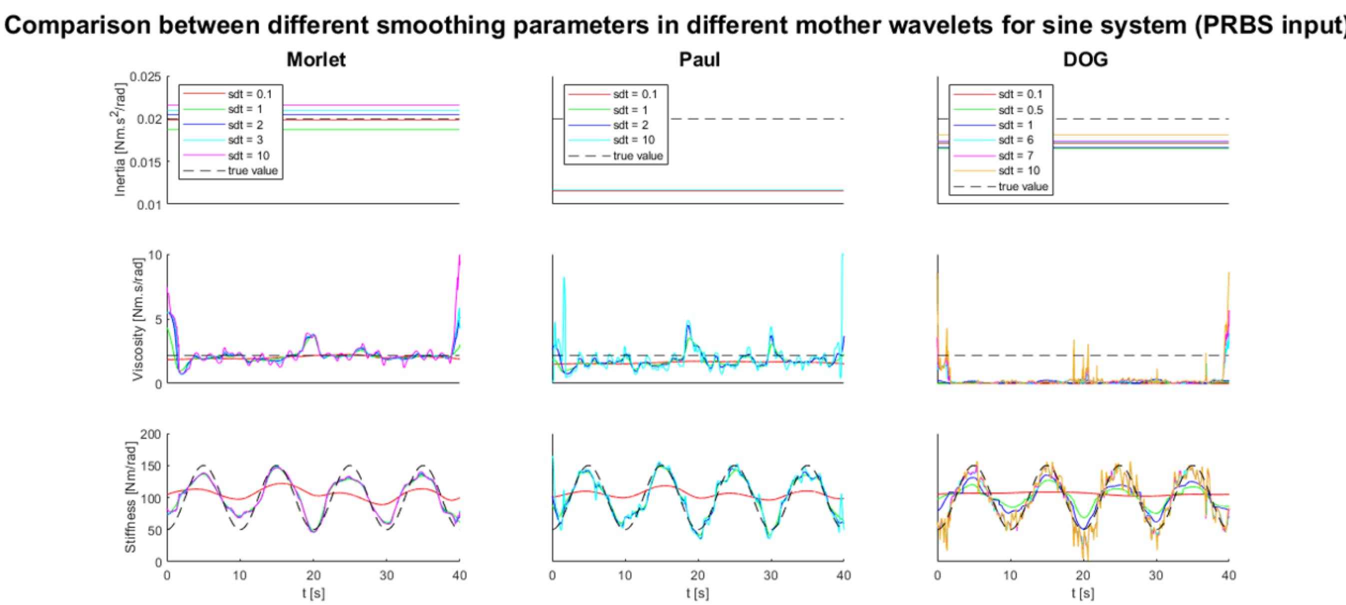

Fig. 57. The estimated result of the parameters selected. The system to be identified is the sine system with a PRBS as input perturbation.

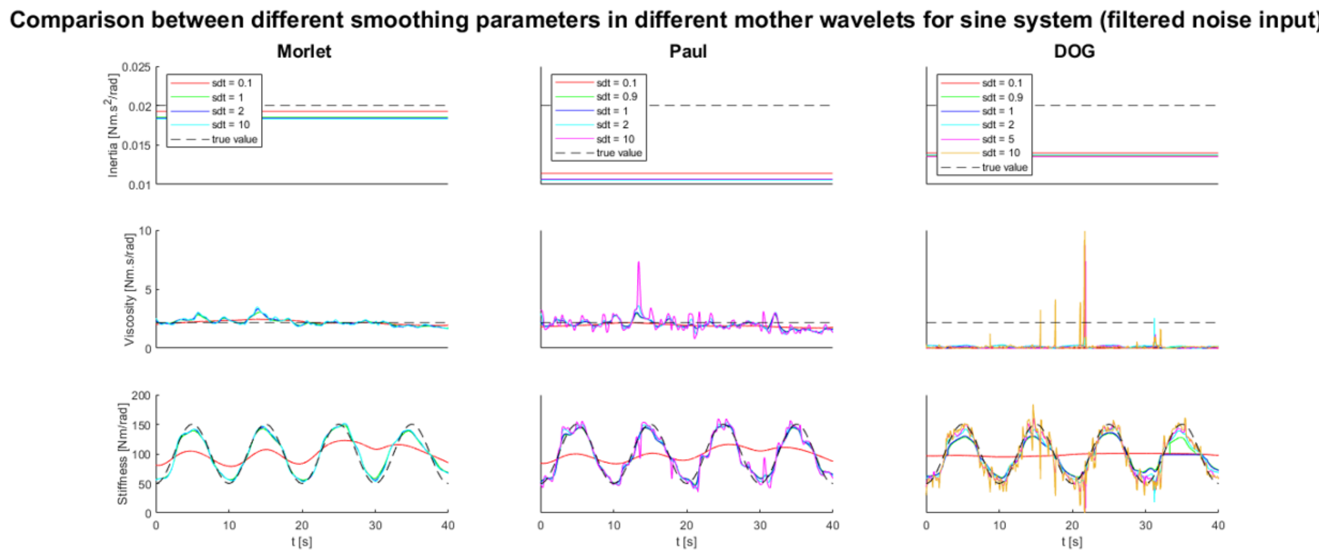

Fig. 58. The estimated result of the parameters selected. The system to be identified is the square system with a filtered noise as input perturbation.

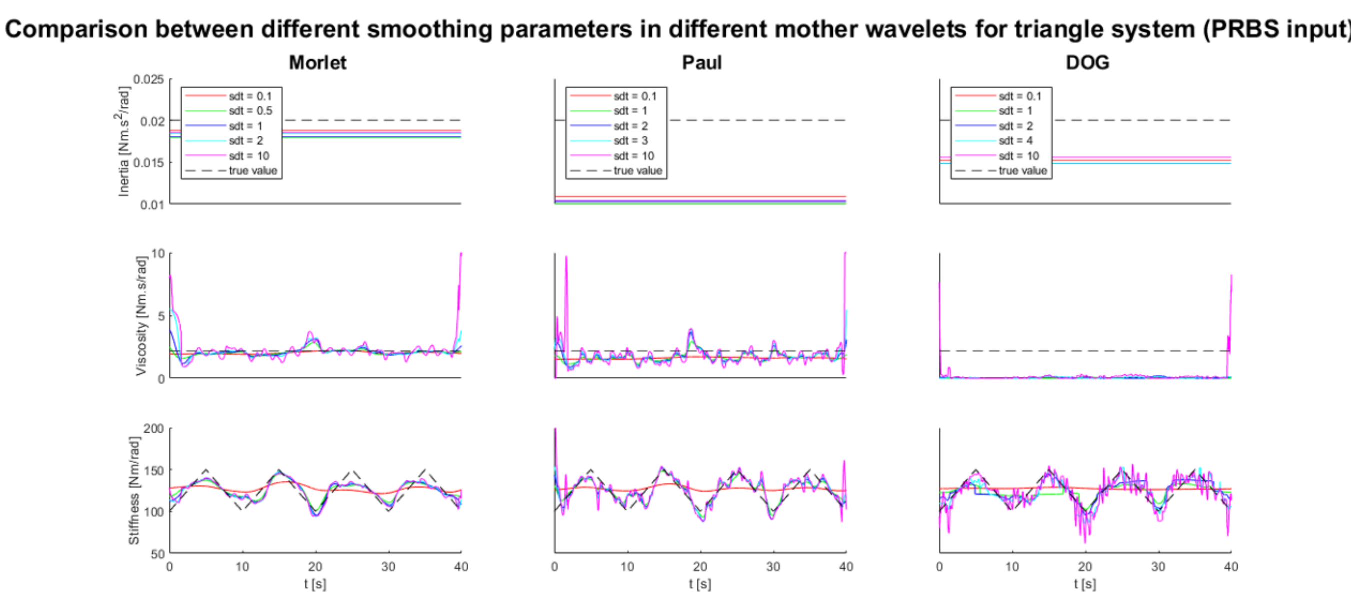

Fig. 59. The estimated result of the parameters selected. The system to be identified is the triangle system with a PRBS as input perturbation.

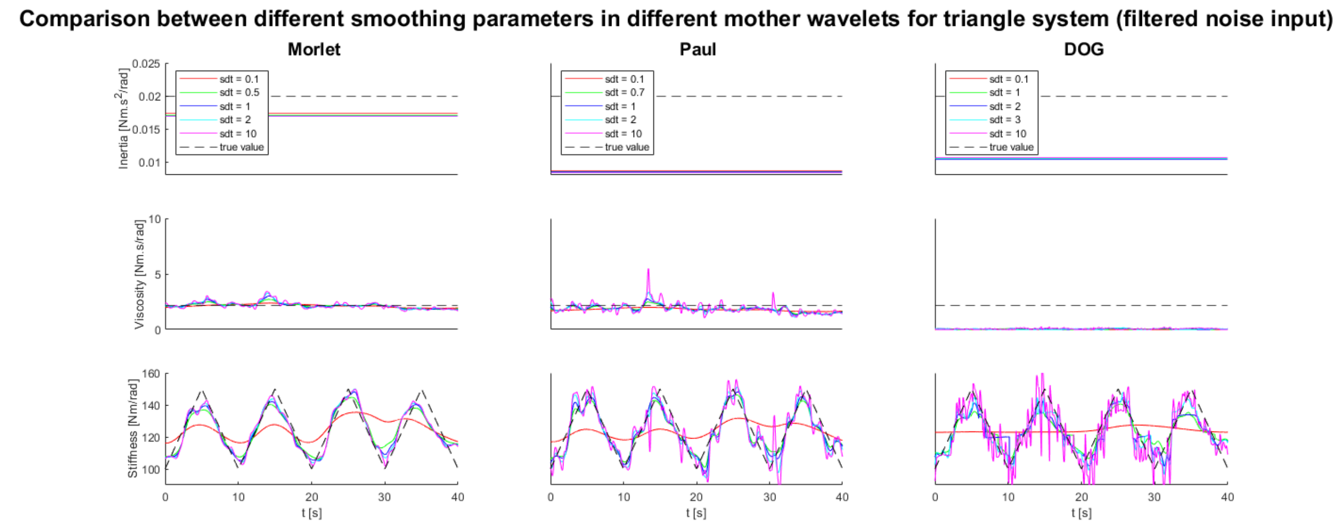

Fig. 60. The estimated result of the parameters selected. The system to be identified is the triangle system with a filtered noise as input perturbation.

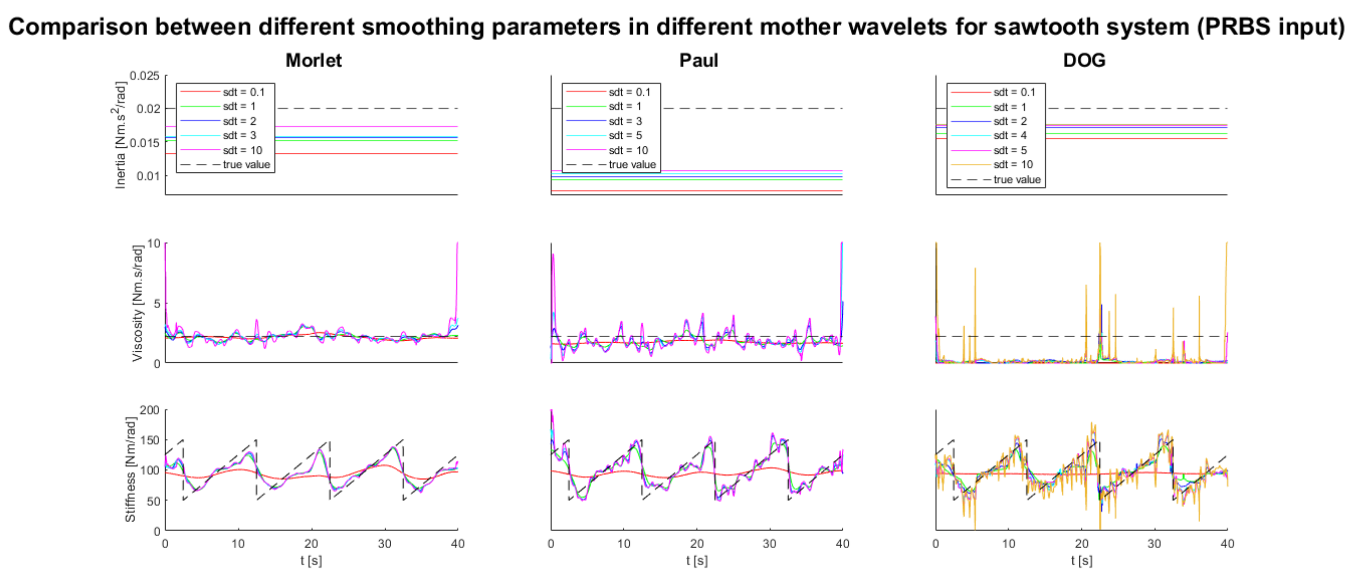

Fig. 61. The estimated result of the parameters selected. The system to be identified is the sawooth system with a PRBS as input perturbation.

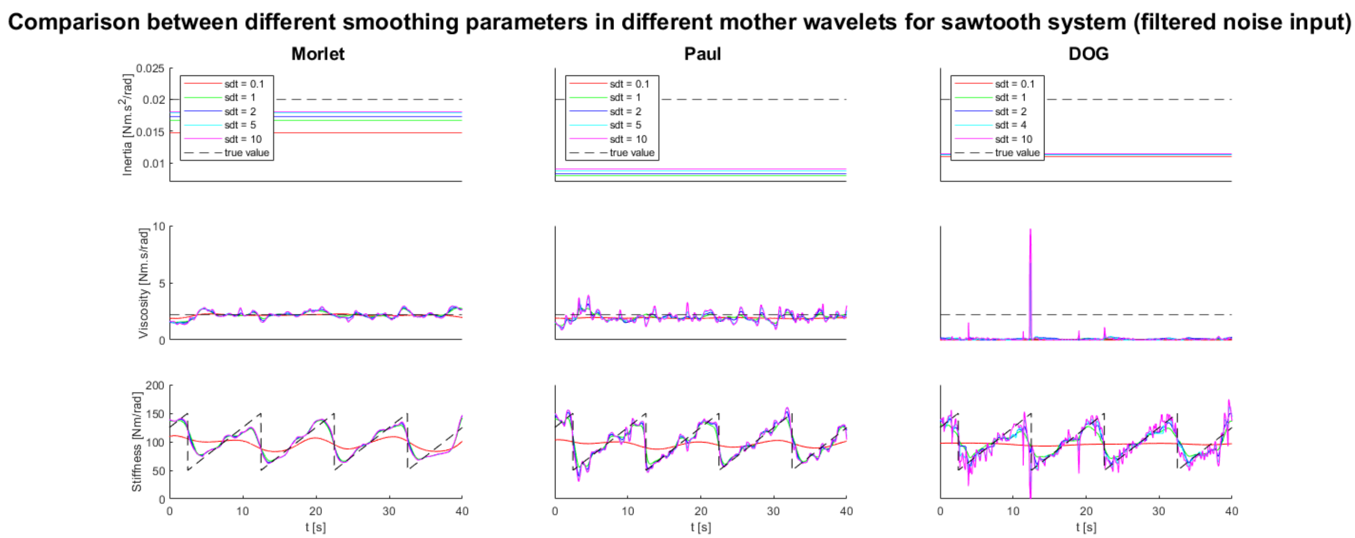

Fig. 62. The estimated result of the parameters selected. The system to be identified is the sawooth system with a filtered noise as input perturbation.